Cross-Modality Neuroimage Synthesis: A Survey

GUOYANG XIE*, Southern University of Science and Technology, China and University of Surrey, United Kingdom

YAWEN HUANG*, Jarvis Research Center, Tencent YouTu Lab, China

JINBAO WANG†, Southern University of Science and Technology, China

JIAYI LYU, University of Chinese Academy of Sciences, China

FENG ZHENG†, Southern University of Science and Technology, China

YEFENG ZHENG, Jarvis Research Center, Tencent YouTu Lab, China

YAOCHU JIN, Bielefeld University, Germany and University of Surrey, United Kingdom

Multi-modality imaging improves disease diagnosis and reveals distinct deviations in tissues with anatomical properties. The existence of completely aligned and paired multi-modality neuroimaging data has proved its effectiveness in brain research. However, collecting fully aligned and paired data is expensive or even impractical, since it faces many difficulties, including high cost, long acquisition time, image corruption, and privacy issues. An alternative solution is to explore unsupervised or weakly supervised learning methods to synthesize the absent neuroimaging data. In this paper, we provide a comprehensive review of cross-modality synthesis for neuroimages, from the perspectives of weakly supervised and unsupervised settings, loss functions, evaluation metrics, imaging modalities, datasets, and downstream applications based on synthesis. We begin by highlighting several opening challenges for cross-modality neuroimage synthesis. Then, we discuss representative architectures of cross-modality synthesis methods under different supervisions. This is followed by a stepwise in-depth analysis to evaluate how cross-modality neuroimage synthesis improves the performance of its downstream tasks. Finally, we summarize the existing research findings and point out future research directions. All resources are available at https://github.com/M-3LAB/awesome-multimodal-brain-image-systhesis.

1 INTRODUCTION

The necessity of cross-modality neuroimage synthesis. The majority of multi-center neuroimaging datasets [3, 89] are often high-dimensional and heterogeneous, which is shown in Fig. 1. For example, positron emission tomography (PET) and magnetic resonance imaging (MRI) are classic medical imaging techniques that provide detailed anatomic and physiological images of different organs for auxiliary diagnosis or monitoring treatments. The paired or registered multi-modality data provide more complementary information to investigate certain pathologies, including neurodegeneration.

---

*The authors contributed equally to this research.
†Co-corresponding authors

MRI CT T1w T2w PET Ultrasound MRI

Transverse Coronal Sagittal

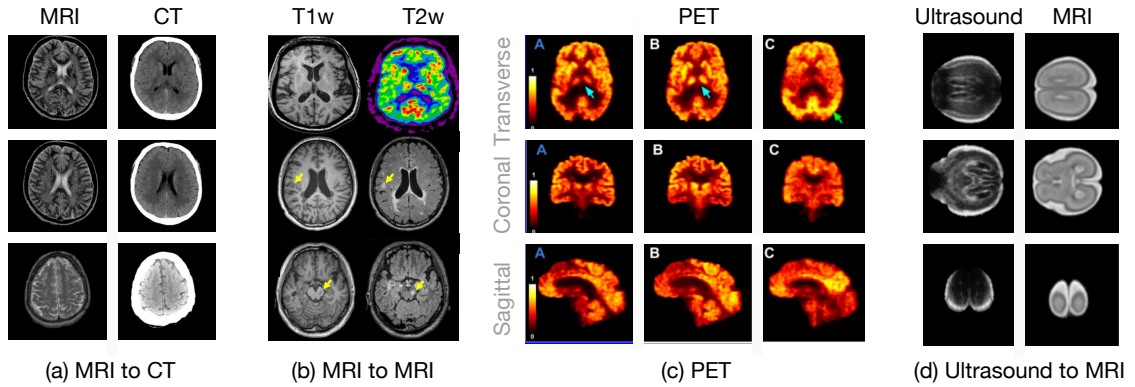(a) MRI to CT (b) MRI to MRI (c) PET (d) Ultrasound to MRI

Fig. 1. Multi-modality synthesis. (a) MRI to CT [25], (b) MRI to PET [123], (c) PET [130], and (d) ultrasound to MRI [48].

However, it is not feasible to acquire a full set of wholly paired and aligned multi-modality neuroimaging data, considering that:

- Collecting multi-modality neuroimaging data is very costly. For example, a normal MRI can take more than one thousand dollars in some countries;
- Many medical institutions cannot share their data since medical data are predominantly restricted by local regulations, despite that identifiable information can be removed to protect the privacy of patients;
- Patient motions may result in severely misaligned neuroimaging data.

As a result, there is a clear need to handle the absent data through a cross-modality synthesis method.

Cross-modality Generative Adversarial Networks (GANs) in medical imaging community. Previously, the key problems in the medical imaging community were: (1) how to fasten multi-contrast MRI reconstruction, (2) how to enhance the image quality of MRI or computed tomography (CT) scan, (3) medical image registration, and (4) fine-grained medical image segmentation. Experienced researchers can quickly iteratively construct innovative algorithms because the majority of them have rather mature answers, ensuring feasibility and high precision from design to product deployment. Cross-modality neuroimage synthesis algorithms, however, were still in their infancy as of 2018 since the synthesized neuroimage quality could not satisfy radiologist's demands. The situation changed substantially when CycleGAN [132] emerged. As shown in Fig. 2(a), we can easily observe that the number of unsupervised and weakly supervised learning methods is increasing. The researchers have paid more attention to unsupervised and weakly supervised learning methods. Fig. 2(c) indicates the number of downstream tasks with each supervision level. It can be easily observed that most unsupervised and weakly supervised methods are jointly optimized with the segmentation task. However, classification and diagnosis tasks are ignored in unsupervised learning and weakly supervised learning methods, to which we believe future work should pay more attention. Fig. 2(b) presents modality synthesis according to the level of supervision. We notice that most of the algorithms conduct cross-modality synthesis for MRI. However, PET and MRI have not received enough attention in unsupervised learning and weakly supervised learning algorithms. We expect future work to propose a uniform generator to synthesize an arbitrary modality among PET, MRI or CT in an unsupervised or weakly supervised learning manner.

Look back cross-modality neuroimage synthesis. From the evolution standpoint, natural image-to-image translation leads the development of cross-modality neuroimage synthesis. Inspired by *dictionary learning* [1], Roy *et*
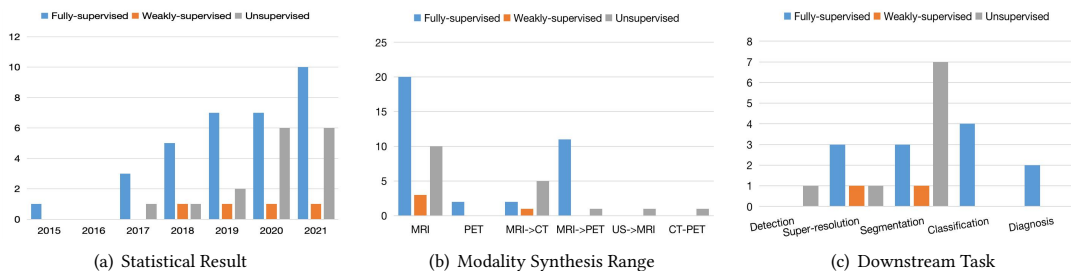
Fig. 2. Trend of each learning manner in multi-modality brain image synthesis literature. (a) The number of papers published chronologically for different levels of supervision papers. (b) The distribution of modality synthesis mode according to the level of supervision. (c) The number of various downstream tasks according to the level of supervision.

al. [81] trained two dictionaries where the input image is used to find similar patches in a source modality dictionary and the corresponding target modality counterpart will be extracted from the target dictionary to generate the desirable modality data. The work of Huang *et al.* [37] improves the quality of cross-modality synthesis by imposing a graph Laplacian constraint in a joint dictionary learning framework. Wang *et al.* [96] synthesizes the missing DT images from T1-w scans by learning a region-enhanced joint dictionary. When *pix2pix* [46] was released in 2017, the situation drastically changed. Most supervised cross-modality neuroimage synthesis algorithms adopt variants of pix2pix. Maspero *et al.* [67] directly employ pix2pix to synthesize CT scans from MRI. The work of Olut *et al.* [74] synthesizes magnetic resonance angiography (MRA) from T1 and T2 with the addition of a steerable filter loss on pix2pix. Furthermore, *CycleGAN* [132] boosts the performance of unsupervised cross-modality neuroimage synthesis. Hiasa *et al.* [31] employ gradient consistency loss to optimize the edge map of the synthesized neuroimage. Zhang *et al.* [127] propose two segmentation networks to segment the corresponding image modality into semantic labels and provide implicit shape constraints on the anatomy during translation. Chen *et al.* [10] propose a similar method to the work of Zhang *et al.* [127]. The only difference between them is that the segmentation network of Chen *et al.* [10] is trained offline and fixed during the training phase of the image translation network. ***The inherent properties of medical images are ignored even though natural image-to-image translation approaches reveal many insights into cross-modality neuroimage synthesis.*** For instance, Fig. 3 shows a failed case of CycleGAN [132] for cross-modality neuroimage synthesis. In particular, the lesion region of the target modality (red box of Fake A) cannot be accurately synthesized in comparison to the lesion region of the source modality (red dashed box of Real B), particularly for the structural details. Therefore, it is necessary to investigate more deeply to characterize the network architecture for the imaging principle of neuroimages.

Motivation and objectives. In recent years, unsupervised cross-modality synthesis has garnered a growing amount of attention, and a number of practical solutions have been proposed to tackle this complex problem. There is no systematic review of the current state of cross-modality neuroimage synthesis, particularly for unsupervised methods and their application in downstream tasks. The primary objective of this survey is to provide a comprehensive study on cross-modality neuroimage synthesis and a solid foundation for newcomers interested in this field and related topics. This paper offers a comprehensive summary of the state-of-the-art cross-modality neuroimage synthesis methods. In addition, we investigate in depth how to use cross-modality neuroimage synthesis for tasks such as tumor segmentation, lesion detection, and diagnosis. Finally, the remaining open questions for future research are discussed.
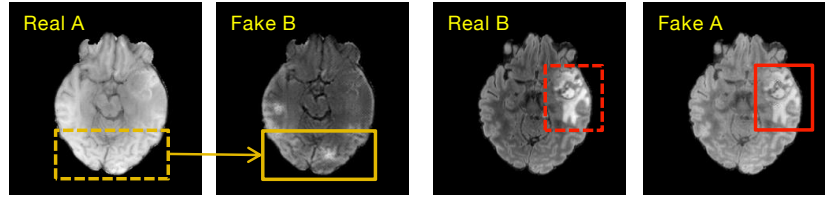
Fig. 3. A failed case in multi-modality brain image synthesis. In addition to generating low-resolution images, another problem is that the disease-related regions cannot be synthesized well. For example, when the target modality (Fake B) is generated from the input real modality (Real A), there exist failed regions (box) that are learned from the original ones (dashed box).

Table 1. Comparison on related surveys in terms of supervision level, modality synthesis mode and downstream tasks.

Survey	Supervison Level			Modality Synthesis Mode					Downstream Tasks			
	Fully-	weakly-	Un-	MRI→MRI	PET→PET	MRI→CT	US→MRI	CT→PET	Segmentation	Classification	Registration	Diagnosis
Yi *et al.* [115]	✔			✔	✔	✔		✔				
Zhao *et al.* [128]	✔			✔					✔	✔	✔	✔
Ours	✔	✔	✔	✔	✔	✔	✔	✔	✔	✔	✔	✔

Comparison to existing surveys. Table 1 compares the present survey with two existing ones concerning the level of supervision, the range of modality synthesis, and the downstream task. The work of [115] provides a comprehensive review of generative adversarial networks (GANs) in medical imaging before 2019, including single-modality synthesis, cross-modality synthesis, and the usage of the GAN in different downstream tasks, e.g., classification, segmentation, registration. However, this work is different from previous reviews [115, 128] in three aspects: (1) The work [115] was published in 2019, where most of the cross-modality synthesis methods reviewed [115] are supervised. In other words, most synthesis algorithms require fully paired medical data for training. (2) The performance of the downstream tasks when leveraging the synthesized results is missing in the review, which is of great importance since the final purpose of cross-modality synthesis serves as an auxiliary procedure for the downstream tasks, e.g., segmentation. Another work in [128] comprehensively reviews the state-of-the-art deep learning-based methods applied to brain MRI, including segmentation, registration, and diagnosis. It touches upon cross-modality brain synthesis but does not go into detail. Furthermore, a review of the taxonomy is presented in [128], which focuses on the task without considering the level of supervision. In addition, it reviews brain magnetic resonance imaging-related work, mainly ignoring other common imaging modalities such as CT and PET. (3) Our review offers a comprehensive analysis and in-depth understanding of the loss function and evaluation metrics. The loss function is classified into three streams based on its function in cross-modality neuroimage synthesis. Furthermore, our study extensively examines the limitations of current metrics and provides insight into the future route to evaluate the quality of synthesized neuroimages.

Contributions. The main contributions of this survey paper can be summarized as follows:

- To the best of our knowledge, it is the first work to provide an in-depth review of cross-modality brain image synthesis by considering the level of supervision, especially for both unsupervised and weakly supervised cross-modality synthesis.
- It provides a comprehensive review of the relationship between cross-modality synthesis and its downstream tasks. This survey focuses on how to synthesize appropriate cross-modality brain images to improve downstream tasks, such as image segmentation, registration, and diagnosis.

- It summarizes the main issues and potential challenges in cross-modality brain image synthesis, highlighting the underlying research directions for future work.

Organization. The rest of the paper is organized as follows. We begin with a chronological overview of cross-modality brain image synthesis and review these methods in Section 2. In Section 3.1, we review cross-modality neuroimage synthesis on the basis of the level of supervision. Next, we review recent advances in modality synthesis in Section 3.2. In Section 3.3, we provide an analysis of how cross-modality synthesis significantly improves the performance of the downstream tasks. Then, in Section 4.1, we describe the popular datasets and go over various loss functions in Section 4.2 and take a retrospective view of the evaluation metrics in Section 4.3. In the end, we provide future research directions for brain neuroimage cross-modality synthesis in Section 5.

2 CHRONOLOGICAL REVIEW

Fig. 4 gives a chronological overview of the cross-modality brain synthesis methods according to the level of supervision, the relevant downstream tasks, and the mode of modality synthesis. In 2013, Roy *et al.* [81] was the first to introduce the dictionary method [111] into cross-modality neuroimage synthesis. Ye *et al.* [114] propose a modality propagation method and prove that the proposed model can be derived from the generalization of label propagation strategy [28], and show applications to arbitrary modality synthesis. In 2015, Nguyen *et al.* [72] trained a location-sensitive deep network to integrate intensity features and spatial information, more accurately synthesizing the results for the same problem posed by [114]. In 2017, the works in [38, 50, 73] introduced cross-modality brain image synthesis into the medical GAN community. Their methods are supervised, i.e., their training data are fully paired. Huang *et al.* [38] construct a closed loop filter learning strategy to learn the convolutional sparse coding (CSC), which can eliminate the requirement of large-scale training data. Meanwhile, it is also the first to undertake super-resolution and multi-modality neuroimaging data in MRI. The authors of [50] propose a multi-modality invariant latent embedding model for synthesis. The purpose of this method is to utilize the mutual information from multi-modality maximally and fuse them into the generated image. Nie *et al.* [73] introduce a synthesis method by translating brain MRI data to CT. The authors incorporate the detailed information from brain MRI into the GAN model to generate the brain CT. After that, Huang *et al.* [39] provide a weakly supervised learning approach to cross-modality brain image synthesis. The work in [39] regards the unpaired data as auxiliary resources. They propose a hetero-domain image alignment method to enforce the correspondence for unpaired auxiliary data, which can directly substantiate the benefits of the combination with a few paired data and massive unpaired data. Chartsias *et al.* [9] firstly propose a unified generator model for various MRI modalities. Huo *et al.* [44] firstly apply an unsupervised learning method to cross-modality brain image synthesis. In other words, the multi-modality training data are unpaired. Specifically, they adopt CycleGAN [132] to generate the target modality from the source modality.

After that, the authors in [44] leverage both the synthesized and source modality data for segmentation. It is also the first to employ unsupervised learning methods for downstream tasks. Wei *et al.* [105] provide a complex synthesis approach to synthesize from MRI image to PET image. Specifically, Sketcher-Refiner GANs proposed by [105] decompose the synthesis problem as a sketch-refinement process, in which the sketchers generate the preliminary anatomical and physiological information, and the refiner refines the structure of tissue myelin content. Pan *et al.* [77] provide a method to optimize the cross-modality synthesis and diagnosis tasks jointly. They design a disease-image-specific network (DSNet) by feeding the features generated from the disease-image-specific network into feature-consistency GANs (FC-GANs) to generate the target domain neuroimaging data. Since DSNet is closely associated with FC-GANs,
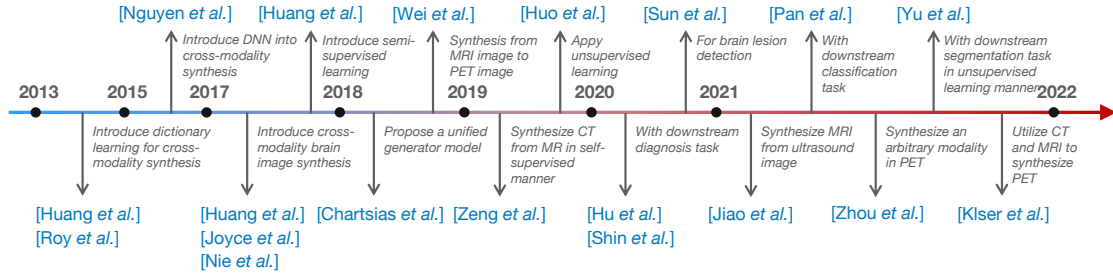
Fig. 4. A chronological review of multi-modality brain image synthesis.

the missing target domain data can be synthesized in a diagnosis-oriented manner. Hu *et al.* [34] and Shin *et al.* [87] are the first to utilize the synthesized neuroimaging data to improve the performance of a classification task. Zhou *et al.* [130] propose a generator to synthesize an arbitrary modality in PET. Klser *et al.* [52] utilize two modalities of data, i.e., CT and MRI, to synthesize PET data. Yu *et al.* [118] jointly optimize the synthesis and segmentation problems using unsupervised learning methods. Jiao *et al.* [48] synthesize MRI from ultrasound image using a new fusion scheme to utilize various modalities from unpaired data. Zeng *et al.* [121] synthesize CT from MR by using self-supervised methods.

3 METHODS

Table 2 and Table 3 provide a taxonomy for the work covered in this survey. Specifically, the second column in the tables is the proposed architecture. The third column denotes the level of supervision, i.e., fully supervised (F), weakly supervised (W), or unsupervised (U) manner. The fourth through sixth columns indicate the loss function, the metrics employed, and whether the input neuroimage images are aligned or misaligned, respectively. The last column refers to the downstream task (DST), which contains super-resolution (SR), segmentation (S), classification (C), detection (D), inpainting (I), registration (R), explainability (E), and diagnosis (Diag). We will discuss each of them in the following sections.

3.1 Learning Paradigms

3.1.1 Fully supervised methods. Before 2018, most synthesis algorithms adopted the CSC filter [120] for dictionary learning-based methods. Previously, dictionary learning [66] was one of popular models for inverse problems in image de-noising [19, 21], image super-resolution [110, 111] and image synthesis [35, 100]. For instance, Elad *et al.* [17] provide a concise overview of sparse and redundant representation modeling and identify ten important future research directions for sparse coding. Rubinstein *et al.* [82] explicate the dictionary acquisition process through mathematical models. Gao *et al.* [20] develop a hypergraph Laplacian matrix to retain the local information of the training samples, thereby enhancing the discriminative capacity of the learned dictionary. Li *et al.* [59] employ the locality information to improve the representative ability of the shared dictionary. Chen *et al.* [15] provide an overview of algorithms on sparse representation learning algorithms focusing on visual recognition. However, the major drawback of CSC is that it requires a huge amount of paired data for training. The work in [38, 39] employs a dual filter training strategy and hetero-domain image alignment to significantly reduce the requirement of a huge amount of paired data. When pix2pix was released in 2017, an alternative generative model, GAN, became mainstream for cross-modality neuroimage

Table 2. A brief summary of cross-modality brain image synthesis methods across different MRI contrast or from MRI to CT. Note that there are three levels of supervision (Sup.), i.e., fully supervised (F), weakly supervised (W) and unsupervised (U). The downstream tasks (DST) contains super-resolution (SR), segmentation (S), detection (D), inpainting (I) and registration (R).

Publication	Name/Arch.	Sup.	Loss/Method	Dataset	Metrics	Align	DST
			$MRI \rightarrow MRI$				
Huang et al. [41]	WEENIE	W	Sparse coding	IXI, NAMIC	PSNR, SSIM	✓	SR
Huang et al. [38]	DOTE	F	Sparse coding	IXI, NAMIC	PSNR, SSIM	✓	SR
Huang et al. [36]	CoCa-GAN	F	$L_{gan}, L_{edge}, L_{gdl}, L_{tumor}$	BraTS15	PSNR, NMSE, SSIM	✓	
Huang et al. [42]	MCMT-GAN	F	$L_{gan}, L_{cyc}, L_{mani}, L_{fault}$	IXI, NAMIC	PSNR, SSIM, DSC	✓	S
Huang et al. [40]	WAG	W	$L_{spc}, L_{mmd}, L_{gcr}$	IXI, NAMIC	PSNR, SSIM	✓	
Huang et al. [43]	GAN	U	$L_{gan}, L_{cont}, L_{text}, L_{cyc}$	IXI, HCP	PSNR, SSIM	✗	SR, I
He et al. [26]	Autoencoder	U	L_{ae}, L_{oth}	IXI	MSE, SSIM	✗	
Yang et al. [109]	Hyper-GAN	U	$L_{gan}, L_{cyc}, L_{rec1}, L_{iden}, L_{cla}$	IXI, BraTS19	PSAR, SSIM, MAE	✗	
Sun et al. [91]	ANT-GAN	U	L_{gan}, L_{cyc}, L_{am}	BraTS18	P, R, F1S, VS	✗	S, D
Guo et al. [23]	CG-SAMR	U	$L_{gan}, L_{fm}, L_{sc}, L_{cm}, L_{rec1}, L_{cyc}$	D5	DSC	✗	S
Shen et al. [86]	ReMIC	W	$L_{gan}, L_{cyc}, L_{rec1}, L_{dice}$	BraTS18, ProstateX	NRMSE, PSNR, SSIM	✗	S, I
Tomar et al. [92]	SASAN	U	$L_{sgan}, L_{cyc}, L_{iden}, L_{reg}, L_{dice}$	BraTS15	DSC, ASSD	✗	S
Charsias et al. [9]	Autoencoder	F	L_{ae}	ISLES15, BraTS15, IXI	MSE, PSNR, SSIM	✓	
Chen et al [12]	ABCNet	F	$L_{gan}, L_{sm}, L_{liu}, L_{cor}$	BCP, dHCP, HCP	DSC, ASSD, CC, CIV, HD95	✓	
Bône et al. [7]	Autoencoder	F	L_{rec2}	–	PSNR, SSIM, L2, t-L2		
Dar et al. [16]	pGAN	F	$L_{cgan}, L_{p2p}, L_{prec}, L_{cyc}$	MIDAS, IXI, BraTS15	PSNR, SSIM	✗	
Jog et al. [49]	REPLICA	F	Random forest	MMRR	PSNR, SSIM, UQI	✓	
Joyce et al. [50]	Autoencoder	F	L_{p2p}	ISLES15, BraTS15	MSE	✗	
Kwon et al. [55]	Autoencoder	F	L_{gan}	ANDI, BraTS18, ATLAS	MMD, MSSSIM	✓	
Qu et al. [80]	MCGAN	U	$L_{gan}, L_{ssim}, L_{rec2}, L_{cyc}, L_{edge}$	BraTS15	PSNR, SSIM, DSC	✓	S
Lee et al. [57]	CollaGAN	F	L_{gan}, L_{ssim}	D9	NMSE, SSIM	✓	
Li et al. [58]	DiamondGAN	F	L_{rec1}, L_{gan}	D10	PSNR, MAE	✗	
Liu et al. [62]	Conditional GAN	F	L_{gan}, L_{p2p}, L_{mc}	BraTS18	L1, SSIM, PSNR, IS	✓	S
Sharma et al. [85]	MM-GAN	F	L_{lsgan}, L_{p2p}	ISLES15, BraTS18	MSE, PSNR, SSIM	✓	
Xin et al. [107]	TC-MGAN	F	$L_{gan}, L_{p2p}, L_{cls}, L_{seg1}$	BraTS18	PSNR, SSIM	✓	
Yang et al. [112] [113]	cGANs	U	L_{cgan}, L_{rec1}	MRBrainS13, ANDI, RIRE, iSeg17, BraTS15	MAE, PSNR, MI, F-score, DSC	✓	S, R
Yu et al. [117]	SA-GAN	F	L_{gan}, L_{iden}	BraTS15, SSIS15	PSNR, NMSE, SSIM	✓	
Yu et al. [116]	3D cGAN	F	L_{cgan}, L_{iden}	BraTS15	PSNR, NMSE, DSC	✓	S
Yurt et al. [119]	mustGAN	F	L_{cgan}, L_{iden}	IXI, ISLES15	PSNR, SSIM	✓	
Zhou et al. [131]	Hi-Net	F	L_{cgan}, L_{rec1}	BraTS18, ISLES15	PSNR, SSIM, NMSE	✓	
Zuo et al. [133]	DMC-Fusion	F	L_{rec1}, L_{ssim}	D15	MI, Q, FMI, PSNR, SSIM	✓	
Bian et al. [6]	DDA-Net	U	$L_{gan}, L_{cyc}, L_{seg}$	MRBrainS18	DSC, SEN, SPE, ROC	✓	S
			$MRI \rightarrow CT$				
Hemsley et al. [29]	cGAN	W	L_{cgan}, L_{p2p}	D1	MAE	✓	
Huo et al. [44]	SynSeg-Net	U	$L_{gan}, L_{cyc}, L_{seg}$	D3	DSC, ASD	✗	S
Yang et al. [108]	sc-cycleGAN	U	L_{lsgan}, L_{cyc}	D6	MAE, PSNR, SSIM	✗	
Zeng et al. [121]	2D-cGAN	U	$L_{sgan}, L_{cyc}, L_{rec1}$	D7	MAE, PSNR	✗	
Klser et al. [52]	pCT	U	L_{rec2}	D8	MAE	✓	
Nie et al. [73]	GAN	U	L_{gan}, L_{gdl}	ANDI	PSNR, MAE	✓	
Zuo et al. [133]	DMC-Fusion	F	L_{rec1}, L_{ssim}	D15	MI, Q, FMI, PSNR, SSIM	✓	
Huynh et al. [45]	–	F	Random forest	ANDI	MAE, PSNR	✓	

synthesis [88, 101]. Zhou et al. [131] pay more attention to the layer-wised fusion strategy from multiple input modalities and design a Mixed Fusion Block (MFB) to combine the latent representation from each source modality. Kwon et al. [55] apply the alpha-GAN to generate a 3D brain MRI from a random vector. Huang et al. [36] project multi-modality brain MRI data into one common feature space and utilize the modality invariant information represented in the common feature space to generate the missing target domain image space. After that, they apply gradient-weighted class activate mapping (GradCAM) [84] to interpret why the synthesized neuroimages could be utilized for potential clinical usage. Yurt et al. [119] utilize multi-modality neuroimaging data and fuse their features to generate the target domain data. Jog et al. [49] adopt a multi-scale feature extraction scheme and feed the features to three random forest trees to predict the corresponding area of the target modality. CollaGAN is proposed by [57], which utilizes the invariant embedding features from multi-modality data and fuses their information to synthesize the target modality data.

Table 3. A brief summary of cross-modality brain image synthesis methods for PET synthesis and US → MRI. Note that there are three levels of supervision (Sup.), i.e., fully supervised (F), weakly supervised (W) and unsupervised (U) manner. Downstream task (DST) contains super-resolution (SR), classification (C), detection (D), inpainting (I), registration (R), explainability (E), and diagnosis (Diag).

Publication	Name/Arch.	Sup.	Loss/Method	Dataset	Metrics	Align	DST
			$MRI \rightarrow PET$				
Wang *et al.* [101]	LA-GANs	F	L_{cgan}, L_{p2p}	D2	PSNR	✔	SR
Hu *et al.* [34]	Bidirectional GAN	F	$L_{gan}, L_{rec1}, L_{prec}, L_{kl}$	ADNI	PSNR, SSIM	✔	
Hu *et al.* [33]	BMGAN	F	$L_{gan}, L_{rec1}, L_{prec}, L_{kl}$	ADNI	MAE, PSNR, MSSSIM, FID	✔	
Liu *et al.* [63]	JSRL	F	$L_{gan}, L_{rec1}, L_{cls}$	CLAS, ADNI, AIBL	AUC, BAC, SEN, SPE, F1S	✔	C
Pan *et al.* [76]	LM³IL	F	L_{gan}, L_{cyc}	ADNI	ACC, SEN, SPE, F1S, MCC, AUC	✔	C
Pan *et al.* [75] [77]	FGAN	F	L_{gan}	ADNI	MAE, SSIM, PSNR, AUC, ACC, SPE, SEN, F1S, MCC	✔	C
Shin *et al.* [87]	GANDALF	F	$L_{cgan}, L_{p2p}, L_{cls}$	ADNI	ACC, P, R	✔	C
Wei *et al.* [105]	Sketcher-Refiner GAN	F	L_{cgan}, L_{rec1}	D13	DVR	✔	
Zuo *et al.* [133]	DMC-Fusion	F	L_{rec1}, L_{ssim}	D15	MI, Q, FMI, PSNR, SSIM	✔	
Kao *et al.* [51]	ESIT	U	L_{rec1}	ANDI	MAE, PSNR, SSIM	✔	E
Zhang *et al.* [122]	BPGAN	F	$L_{gan}, L_{rec1}, L_{kl}$	ANDI	MAE, PSNR, SSIM	✔	Diag
			$CT \rightarrow PET$				
Klser *et al.* [52]	pPET	F	L_{rec2}	D8	MAE	✔	
			$US \rightarrow MRI$				
Jiao *et al.* [48]	GAN	U	L_{gan}, L_{p2p}	D4	MOS, DS	✗	
			$PET \rightarrow PET$				
Wang *et al.* [102]	LA-GANs	F	L_{gan}, L_{rec1}	D11, D12	PSNR, SSIM	✔	SR
Zhou *et al.* [130]	UCAN	F	$L_{gan}, L_{iden}, L_{cls}, L_{cyc}$	D14	NMSE, SSIM	✔	Diag

However, supervised cross-modality neuroimage synthesis algorithms are challenging for a product launch because they need many neuroimage data pairs for training, which is tough to get at medical institutions owing to patients' privacy concerns.

3.1.2 Weakly supervised methods. We categorize weakly supervised cross-modality neuroimage synthesis algorithms into two streams. As illustrated in Fig. 5, the first stream is to utilize a cross-modality segmentation mask to extract the knowledge from the lesion region [86]. Then, the knowledge from the segmentation mask is distilled into the generator. In other words, the segmentation network was treated as a teacher to guide the generator using unpaired training data. This method is a potential solution to the problem described in Fig. 3. Since this method transfers the knowledge from the lesion region to the generator, it is possible to make the generator pay more attention to the lesion region and synthesize a high-fidelity neuroimage. The second stream [40, 41] aims to make use of a few paired neuroimaging datasets at first and extract the feature from each modality [125]. BMVC proposed by Zhang *et al.* [125] is the first comprehensive work to encode the multi-view image descriptors into a common feature space and clusters via a binary matrix factorization model. Inspired by this, Huang *et al.* [40] project each modality's feature points into the common feature space and adopt maximum mean discrepancy (MMD) to calculate the divergence of paired feature points in the reproducing common feature space. Ultimately, the new feature from the incoming unpaired source modality neuroimage data employs MMD to seek the intrinsic paired feature points in the common feature space. The new target modality neuroimage is generated by feeding the pair feature points from the common feature space into the generator. The flowchart of the second stream method is given in Fig. 6.

3.1.3 Unsupervised methods. The mainstream for unsupervised cross-modality neuroimage synthesis is CycleGAN [132]. In Fig. 7, CycleGAN is separated into two loops. The first loop is source domain→ synthesized target domain→ reconstructed source domain. The second loop is target domain→ synthesized source domain→ reconstructed target domain.
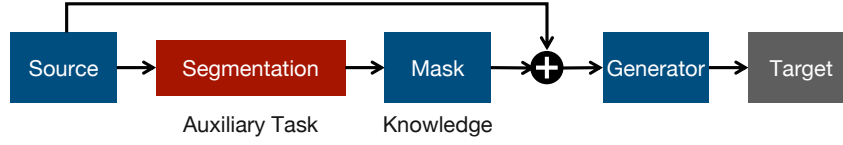
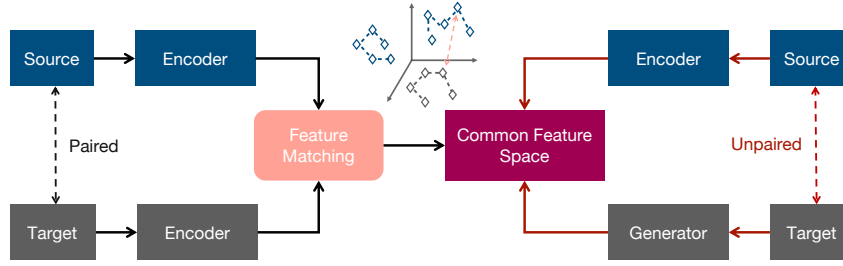Fig. 5. Weakly supervised architecture with an auxiliary task.

Fig. 6. Weakly supervised architecture via projecting into the common feature space.
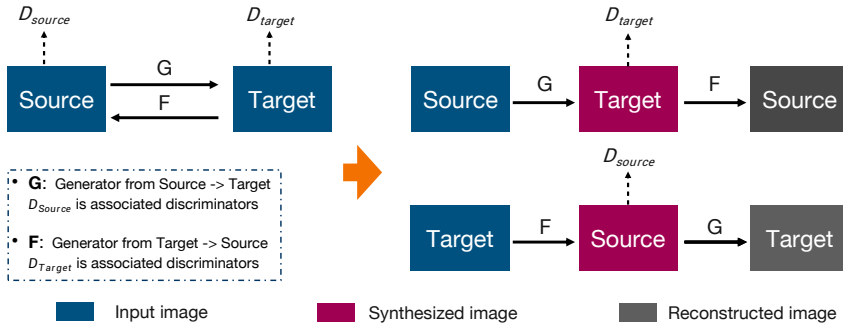

Fig. 7. CycleGAN [132] architecture.

CycleGAN [132] utilizes two loops to construct a cycle loss function, which is described below:

$$\mathcal{L}_{cycle} = \mathbb{E}_{\mathbf{X} \sim p_r(\mathbb{X})} \left\| \mathbf{X} - F(G(\mathbf{X})) \right\|_1 + \mathbb{E}_{\mathbf{Y} \sim p_r(\mathbb{Y})} \left\| \mathbf{Y} - G(F(\mathbf{Y})) \right\|_1, \tag{1}$$

where X denotes the source domain and Y denotes the target domain; G and F are the generators for task $X \rightarrow Y$ and task $Y \rightarrow X$. The GAN loss function in CycleGAN [132] is described as below:

$$\begin{aligned}
\mathcal{L}_{adv} = \; & \mathbb{E}_{\mathbf{Y} \sim p_r(\mathbf{Y})} \left[log \, D_G(\mathbf{Y}) \right] + \mathbb{E}_{\mathbf{X} \sim p_r(\mathbf{X})} \left[log \left(1 - D_G(G(\mathbf{X})) \right) \right] \\
& + \mathbb{E}_{\mathbf{X} \sim p_r(\mathbf{X})} \left[log \, D_F(\mathbf{X}) \right] + \mathbb{E}_{\mathbf{Y} \sim p_r(\mathbf{Y})} \left[log \left(1 - D_F(F(\mathbf{Y})) \right) \right].
\end{aligned} \tag{2}$$

Most variants of unsupervised cross-modality synthesis are built on the basis of the cycle loss in Equation 1 and the adversarial loss in Equation 2. Among them, the main difference usually lies in the extraction and alignment of the features [42, 48, 121]. The work presented by Huang *et al.* [42] is one of the classical models.
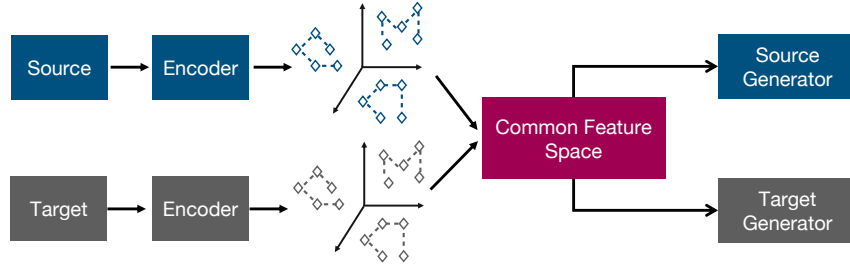
Fig. 8. Unsupervised learning architecture [42] for cross-modality neuroimage synthesis.

In Fig. 8, the unpaired source modality and the target modality neuroimages are fed into the modality-specific feature encoder. Inspired by [79], which is the promising work to seek a shared semantic representation but fully preserve the discriminative modal-specific features, the authors in [42] utilize extended multi-kernel maximum distance to calculate the distance of features from different modalities. If the distance of features is smaller than a particular threshold, MCMTGAN [42] aligns them as paired feature points and constructs a common feature space, which adopts the idea from Zhang *et al.* [126]. In the inference phase, the new unpaired source modality is fed into the modality-specific feature encoder to obtain the reference feature point. Then MCMTGAN seeks the paired feature points of the common feature space. The seek feature paired points are fed into the modality-specific generators to synthesize cross-modality neuroimages. Yu *et al.* [118] present a similar work with the method shown in [42]. However, the authors pay more attention to the mouse brain dataset. Chen *et al.* [11] propose a more concise idea, i.e., the source modality and the target modality share their feature encoder. Jiao *et al.* [48] also extract and map features into the common space using different modalities. Moreover, the authors in [48] design a new cross-modal attention module for fusion and propagation. Zeng *et al.* [121] use two models; one of which is the 3D generator network, and the other is the 2D discriminator. The authors utilize the result from the 2D discriminator treated as a weak label to supervise the 3D generator, such that the generator's output can be closer to the output of CT. Yang *et al.* [109] design a unified generator for MRI synthesis. The method is also similar to [42], which depends mainly on the common feature space. Yang *et al.* [108] also borrow the concept of the common feature space and design a module to make the features from various modalities closer. Tomar *et al.* [92] develop a learnable self-attentive spatial normalization with a GAN, which can significantly improve the generator's performance. He *et al.* [26] treat the synthesis problem as a domain generalization problem. The generator's performance on the unseen target modality cannot be guaranteed due to domain-shift problems.

3.2 Modality Synthesis Mode

3.2.1 MRI contrast synthesis. The upper part of Table 2 shows the review for the synthesis across MRI contrasts, like T1-weighted, T2-weighted, and FLAIR. The synthesis across MRI contrasts is a widely discussed subject within the medical neuroimaging community. In the beginning, Bône *et al.* [7] and Dar *et al.* [16] adopted fully supervised training paradigms for the synthesis across MRI contrasts. Both of them employ autoencoder [95] as their neural network architecture. However, a significant limitation of these methods is their reliance on a substantial quantity of paired neuroimaging data for training, which poses a considerable challenge in acquisition within hospitals or medical centers. In 2018, Huang *et al.* [40] proposed a semi-supervised method for cross-modality neuroimage synthesis, which fully leverages a large number of unpaired neuroimages to construct a feature space and subsequently extracts the features from a limited number of paired neuroimages to regulate the manifold of feature space. The year 2020
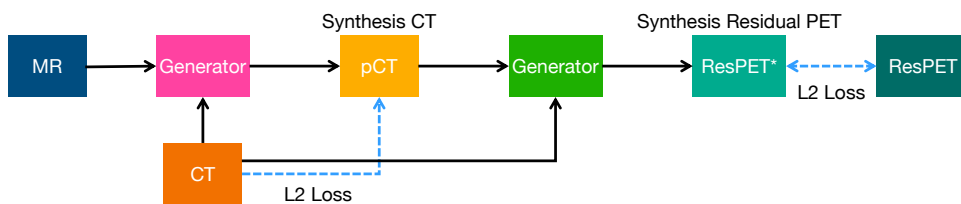
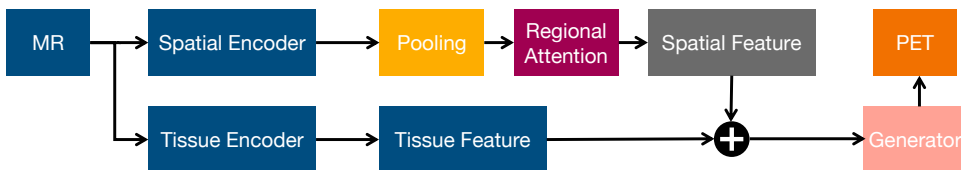Fig. 9. Architecture proposed in [52] for MRI to CT and PET synthesis.

Fig. 10. Architecture proposed in [51] for MRI to PET synthesis.

witnessed the emergence of unsupervised cross-modality neuroimage synthesis [109] in the academia, as a considerable number of researchers began utilizing GAN for cross-modality neuroimage synthesis [91, 92]. For instance, the aim of ANT-GAN [91] is to produce a visually normal neuroimage based on its abnormal counterpart without needing paired neuroimages. Tomar *et al.* [92] employ cross-modality neuroimage synthesis to address domain adaptation issues. Furthermore, Yang *et al.* [109] try to propose a unified GAN model for the synthesis of all modalities, including T1-weighted, T2-weighted and FLAIR. Specifically, the authors of [109] propose a pair of hyper-encoder and hyper-decoder to facilitate the mapping process from the source contrast to a shared feature space, followed by a subsequent mapping to the target contrast image.

3.2.2 MRI To CT. Computed tomography (CT) is of great importance for different clinical applications, such as PET attenuation correction and radiotherapy treatment planning. However, the patients need to be exposed to radiation during CT acquisition, which may cause side effects. Nevertheless, MRI is much safer than CT. Therefore, there is a clear need to synthesize CT [44, 73, 121] from MRI. In Fig. 1(a), the first column denotes MRI, and the second column denotes its paired CT. As shown in Fig 9, one of the classical architectures proposed by [52] constructs two networks. The role of the first network is to generate CT (pseudo-CT) from MRI. The role of the second network is to generate PET from pseudo-CT. The total training process can be divided into two parts. The first part makes pseudo-CT more consistent with the real CT, and the second part aims to make the generated PET more consistent with the real PET. In the first part of the training stage, the authors feed the paired MR and CT into the first generator. The synthesized CT and the real CT construct an L2 loss function to optimize the parameters of the first generator. In the second part of the training stage, the authors feed the synthesized CT and the real CT into the second generator. The synthesized residual PET and the ground truth residual PET formulate an L2 loss function to optimize the parameters of the second generator.

3.2.3 MRI To PET. Positron emission tomography (PET) is an essential measure of myelin content changes in vivo in multiple sclerosis. However, PET imaging is costly and invasive due to the injection of a radioactive tracer. In contrast, MRI is much safer since it is not invasive. Therefore, it significantly motivates the researchers to synthesize PET from MRI [105]. In addition, PET is also regarded as the gold standard for diagnosing Alzheimer's disease (AD). As previously

mentioned, PET can be prohibitive due to its cost and invasive nature. Shin *et al.* [87] propose a conditional GAN to synthesize PET from MRI, where the auxiliary information is from AD diagnosis. Liu *et al.* [63] employ a GAN to synthesize PET from MRI and then feed the generated PET and real MRI into the segmentation. Hu *et al.* [33] employ a bidirectional mapping mechanism to synthesize between MRI to CT. Kao *et al.* [51] lay the explanatory groundwork for the cross-modal medical image translation model by exploring the biological plausibility behind the deep neural network, mainly focusing on the T1-MRI to PET translation, as shown in Fig. 1(b). The architecture details are shown in Fig. 10. The input MRI is fed into two feature encoders. One is the spatial encoder; the other is the tissue encoder. The spatial and tissue features are merged and sent into the generator to synthesize the target PET.
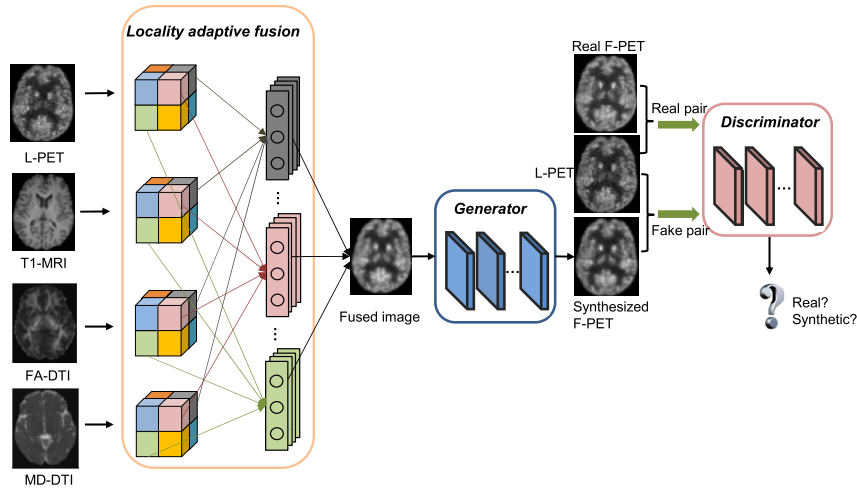

Fig. 11. PET synthesis architecture [102].

3.2.4 PET. Unlike previous methods for one-to-one fixed modality translation, Zhou *et al.* [130] propose a 3D unified Cycle-GAN (UCAN) to synthesize PET, as shown in Fig. 1(c). Another method is proposed by Wang *et al.* [102], which is shown in Fig. 11. They propose a 3D auto-encoder to capture various PET modality features into one common space and then utilize the common feature space for synthesizing arbitrary PET modalities. Specifically, the input neuroimage contains PET, MRI, and DTI modalities. The shared feature encoder extracts the feature from modality-specific neuroimage. Then, the feature maps from different modalities are aligned to generate the fused images via the proposed locality adaptive fusion block. The fused images are fed into the generator to synthesize paired neuroimages of different modalities. The role of the discriminator is to classify whether these synthesized paired neuroimages are real or fake.

3.2.5 Ultrasound to MRI. Ultrasound (US) is the most common method to detect abnormalities in the fetal brain and growth restriction. However, the quality of ultrasound is easily affected by acoustic windows and occlusions, which mainly come from the fetal brain skull. MRI is unaffected by this case and is able to provide more complete spatial details for full anatomy. One major drawback is that the paired data for ultrasound and MRI is tough to collect. Jiao *et al.* [48] employ self-supervised methods to synthesize MRI from ultrasound images, as shown in Fig. 1(d). In Fig. 12, the ultrasound neuroimage and the MRI neuroimage are fed into the modality-specific feature encoder. All features are
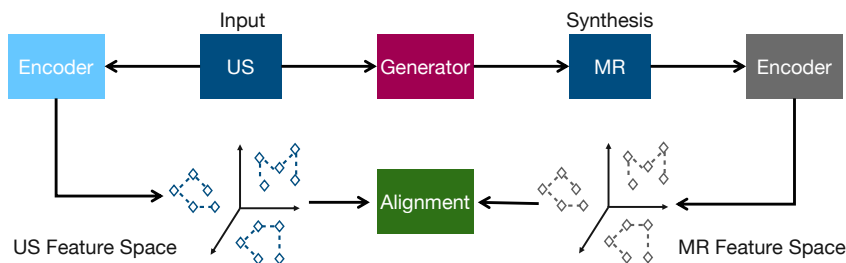
Fig. 12. Architecture purposed in [48] for ultrasound (US) to MRI synthesis.

aligned in one common feature space. The appearance and edge features of MRI and ultrasound are used to constrain the reconstruction process.

3.3 Downstream Tasks

3.3.1 Segmentation. We summarize how the segmentation task is incorporated into cross-modality neuroimage synthesis. In general, there are two categories of methods. The first category aims to utilize cross-modality synthesized neuroimage to improve the performance of the segmentation task. A typical architecture purposed in [86] is shown in Fig. 13. The synthesized target and original source modality neuroimage are concatenated and fed into the segmentation network [44, 86, 118]. Huo *et al.* [44] directly use the accuracy of the segmented results to evaluate whether the synthesized data is helpful without evaluating the quality of the synthesized results by peak signal-to-noise ratio (PSNR) and the structure similarity index (SSIM). Yu *et al.* [118] jointly optimize the synthesis and segmentation tasks using an unsupervised learning method.
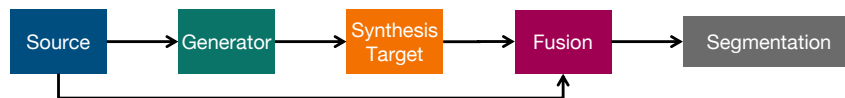
Fig. 13. Architecture purposed in [86], which uses synthesized images to improve the segmentation accuracy.
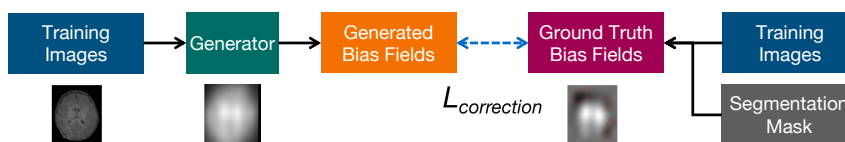
Fig. 14. Architecture purposed in [12], which uses segmentation masks to improve the quality of synthesized images.

Furthermore, the second category aims to utilize a segmentation mask to boost the performance of cross-modality neuroimage synthesis [12, 23, 129]. For instance, the architecture of Chen *et al.* [12] is shown in Fig. 14. To be specific, the training images and the corresponding segmentation masks generate the ground truth bias fields. Then, the synthesis bias fields and the ground truth bias fields formulate a correction loss to optimize the parameters of the generator. Chen *et al.* [12] pay more attention to the brain MRI of infants. The authors incorporate the manual annotations of tissue segmentation maps into the synthesis procedure and make the generated data more segmentation-oriented.

Finally, the work in [12] proves that the synthesized maps can significantly improve segmentation accuracy. Guo *et al.* [23], Shen *et al.* [86] and Zhou *et al.* [129] leverage the segmentation task to guide the synthesis task.

Fig. 15. Architecture purposed in [63] for cross-modality neuroimage synthesis for the downstream classification task.

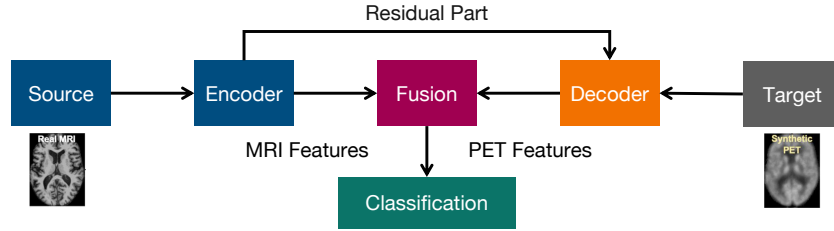*3.3.2   Classification.* In Fig. 15, we summarize how the classification task is incorporated into cross-modality neuroimage synthesis in the method purposed in [63]. The feature embedding from the source modality neuroimage and the feature embedding from the synthesis target modality are mixed as the input for the classification task [34, 63, 87]. Similar to Fig. 15, the work in [87] incorporates AD's information as an auxiliary task to improve the target modality image synthesis performance. Since the synthesis process is classification-oriented, the synthesized brain image can primarily improve the performance of AD's classification. Hu *et al.* [34] design a bidirectional mapping mechanism to preserve the brain structures with high-fidelity details. The work in [34] verifies that the synthesized neuroimaging data can increase the classification accuracy.
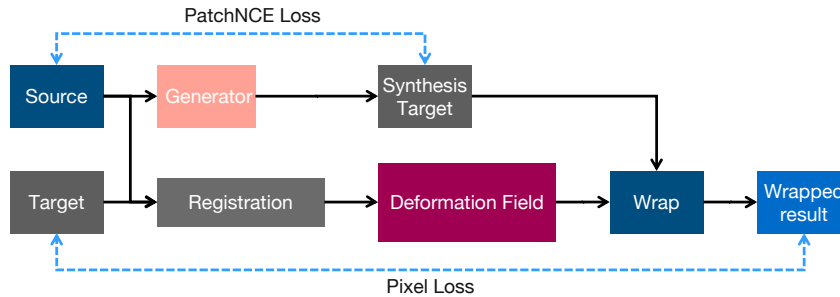
Fig. 16. Architecture proposed in [14] for cross-modality neuroimage synthesis for the downstream registration task.

3.3.3   Registration. Multi-modality neuroimage registration [64] is a traditional topic for the medical imaging community. However, the upcoming trend is utilizing cross-modality neuroimage synthesis for registration [14, 27]. One representative example is given in [14] and its architecture detail is shown in Fig. 16. The model consists of two components. One is the registration network, and the other is the cross-modality synthesis network. Both of them are jointly optimized. The source modality neuroimage is warped to align with the target image via the deformation field. Then, the authors propose a novel PatchNCE loss to preserve the shape information in the synthesized neuroimage. Furthermore, Chen *et al.* [14] employ a pixel-wise reconstruction loss function to preserve the appearance of the synthesis neuroimage. In this case, the proposed model can simultaneously optimize the generator and the registration network.
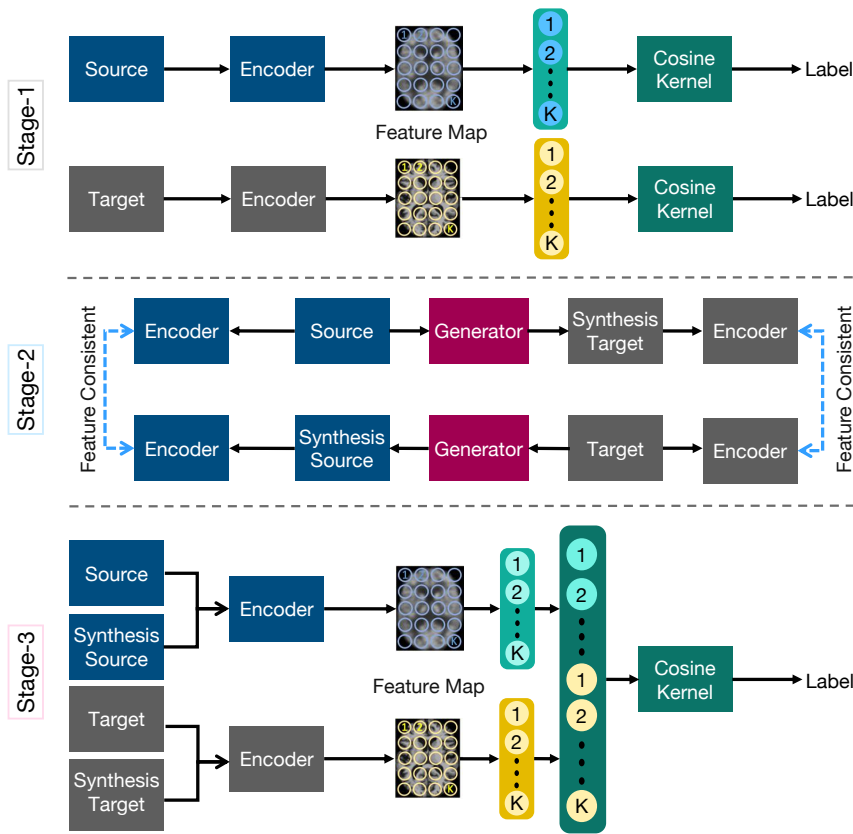
Fig. 17. Architecture proposed in [77] for cross-modality neuroimage synthesis for the downstream diagnosis task [77].

3.3.4 Diagnosis. Pan *et al.* [77] were the first to apply cross-modality neuroimage synthesis to disease diagnosis tasks. The training process is divided into three stages. The architecture details are described in Fig. 17. In the first stage, the input source modality neuroimage and its paired target modality neuroimage are fed into the feature encoder to obtain the modality-specific feature map. They then propose a spatial cosine kernel function to decompose the output feature map into two parts. One is the disease-relevant part, and the other is the residual normal part, which is irrelevant to the disease. The exploited spatial cosine kernel is to ensure that the classifier can learn the disease-relevant features. In the second stage, the source and target feature encoders are frozen. In other words, only the generator is trained in an end-to-end manner. The second stage aims to encourage the feature map from the synthesized neuroimage to be consistent with the feature map from the input neuroimage. In the third stage, the features from the source modality neuroimage and the target modality neuroimage are concatenated for brain disease identification. However, this work adopts a supervised learning method by inputting paired multi-modality neuroimaging data. It is challenging to apply to other tasks since it is very difficult to collect fully paired data.

Table 4. A brief summary of datasets for cross-modality neuroimage synthesis. Note that ♯ and ♮ indicate that it has labels for the segmentation task and classification task, respectively.

Dataset	Subjects	Modality	Data Description
		Public	
IXI	578	MR (T1w, T2w, PDw)	Healthy subjects, 3 hospitals with different acquisition protocols, volume size: $256 \times 256 \times z$ ($z = 112 - 136$). URL: http://brain-development.org/ixi-dataset.
BRATS15 [70]	65♯	MR (T1, T1c, T2, FLAIR)	Multi-contrast MR scans from glioma patients. URL: https://www.smir.ch/BRATS/Start2015.
BRATS18 [8]	285♯	MR (T1w, T2w, FLAIR)	210 high-grade glioma (HGG) and 75 lower grade glioma (LGG) MRI with binary masks for the tumor (or lack of tumor). Each 3D MRI contains 155 slices of size 240×240. URL: https://www.med.upenn.edu/sbia/brats2018.html.
BRATS21	2000♯	MR (T1, T2, FLAIR)	URL: http://www.braintumorsegmentation.org.
NAMIC	20	MR (T1w, T2w)	10 normal controls and 10 schizophrenic, volume size: $128 \times 128 \times z$ ($z = 88$). URL: https://www.na-mic.org/wiki/Downloads.
HCP [94]	200	MR (T1w, T2w)	The Human Connectome Project (HCP), but for healthy young-adult subjects. URL: https://www.humanconnectome.org.
BCP [32]	546	MR (T1w, T2w)	Real infant MRI scans.
ProstateX [61]	98	MR (T2w, ADC, DWI)	Contain 3 modalities: T2w, apparent diffusion coefficient (ADC) and high b-value DWI images.
ISLES15 [65]	65♯	MR (T1w, T2w, FLAIR, DWI)	Ischemic stroke lesion segmentation (ISLES), a medical image segmentation challenge on MICCAI 2015. URL: http://www.isles-challenge.org/ISLES2015.
MIDAS [16]	66	MR (T1w, T2w)	48 subjects for training, 5 for validation and 13 for testing.
ANDI [47]	680♮	MR (T1w), PET	Alzheimer's Disease Neuroimaging Initiative (ADNI). URL: https://adni.loni.usc.edu.
MMRR [56]	21	MR (T2w)	Multimodal Reproducibility Resource (MMRR).
ATLAS [60]	220	MR (T1w)	Anatomical tracings of lesions after stroke (ATLAS), for stroke MRI generation. URL: http://fcon_1000.projects.nitrc.org/indi/retro/atlas.html.
CLAS	76	MR (T1w)	Chinese Longitudinal Aging Study (CLAS).
AIBL [18]	235	MR (T1w), PET	Australian imaging, biomarkers and lifestyle (AIBL) with paired T1w MRI and Flute/PIB-PET scans.
MRBrainS13 [69]	20♯	MR (T1, FLAIR)	URL: https://mrbrains13.isi.uu.nl.
MRBrainS18	7♯	MR (T1, FLAIR)	Providing ground truth labels for 10 categories of brain structures. URL: https://mrbrains18.isi.uu.nl.
iSeg17 [99]	23♯	MR (T1, T2)	661 training images, 163 images for testing.
RIRE [106]	19	MR (T1, T2)	Including T1 and T2 images collected from 19 subjects.
		Private	
D1 [29]	105	MR (T1w, FLAIR), CT	Image size 512×512.
D2 [101]	16	MR (T1), PET	8 normal control subjects and 8 mild cognitive impairment subjects, each with a low-dose PET image, a T1-MRI image and a full-dose PET image. Each aligned image has the resolution of $2.09 \times 2.09 \times 2.03$ mm^3 and the volume size of $128 \times 128 \times 128$.
D3 [44]	60MRI, 19CT	MR (T2w), CT	In total, 3262 MRI slices and 1874 CT slices were used in the experiments.
D4 [48]	107US, 2MRI	MR, US	Around 36,000 2D US slices and 600 MRI slices were extracted accordingly.
D5 [23]	100	MR (T1w, T2w, FLAIR)	Volume size:$256 \times 255 \times 15$, 3 labels: edema; cavity; and tumor.
D6 [108]	45	MR, CT	Training set of 28 subjects, validation set of 2 subjects, and test set of 15 subjects.
D7 [121]	50	MR, CT	2 modalities are aligned with a rigid registration, volume size: $256 \times 288 \times 112$.
D8 [52]	20MRI, 18PET	MR (T1w, T2w), PET	20 pairs of brain MR, CT and 18F-FDG PET images.
D9 [57]	10	MR (T1F, T2w, T2F)	Total 280 axial brain images were scanned and additional T2 FLAIR sequences from 10 subjects. There are four types of MR contrast: T1-FLAIR, T2w, T2-FLAIR, and T2-FLAIR*.
D10 [58]	65	MR (T1, T2, FLAIR, DIR)	65 scans of patients with MS lesions from a local hospital.
D11 [102]	20	MR (T1), PET	20 simulated subjects were generated from the BrainWeb database of twenty normal brains.
D12 [102]	16	MR (T1), PET	8 normal control subjects and 8 mild cognitive impairment subjects, each with L-PET, F-PET, T1-MRI, FA-DTI and MD-DTI.
D13 [105]	18	MR, PET	18 patients (12 women, age 31.4 ± 5.6) and 10 age- and gender-matched healthy volunteers (8 women, age 29.4 ± 6.3).
D14 [130]	35	PET	24 patients diagnosed with AD and 11 patients as healthy control.
D15 [133]	74 pairs	NR (T1, T2), CT, PET	14 pairs of CT/MRI images, 20 pairs of MR-T1/MR-T2, 20 pairs of MR/SPECT, 20 pairs of MR/PET images.
D16 [2]	20	MR, CT	Unpaired brain MR and CT volumes, including 179 two-dimensional (2D) axial MR and CT images.

4 DATASETS, LOSSES AND METRICS

4.1 Datasets

Table 4 presents a summary of the public datasets. It can be easily observed that most public datasets can only be used synthesis for different MRI contrasts (namely, MRI-to-MRI synthesis). There are no datasets for MRI to PET, MRI to CT, or CT to PET synthesis. Most deep-learning models require considerable data to avoid model over-fitting.

Table 5. A brief summary of different losses for cross-modality neuroimage synthesis

Abbr.	Function	Description
L_{gan}	$E_I[\log D(I)] + E_I[\log(1 - D(G(I)))]$	G and D are the generator and discriminator, respectively.
L_{cgan}	$E_{x,y}[\log D(x,y)] + E_{x,z}[\log(1 - D(x, G(x,z)))]$	Learn the transformation from conditioned sample $x \in X$ and random noise vector z to the desired output sample $y \in Y$, $G : \{x, z\} \rightarrow \{y\}$. G and D are the generator and discriminator, respectively, and $E_{a,b}[f(x)]$ is the expected value of $f(x)$ over the distributions of a, b.
L_{sgan}	$E_{y \sim \mathcal{Y}}[D\mathcal{y}(y)^2] + E_{x \sim X}[(1 - D\mathcal{y}(G\mathcal{y}(x)))^2]$	G and D are the generator and discriminator, respectively.
L_{p2p}	$E_{x,y,z}[\|y - G(x,z)\|_1]$	In the context of image-to-image translation, low-frequency information is better captured when an l_1 penalty $\|y - G(x,z)\|_1$ is added to the loss function.
L_{cont}	$E_{x \sim p}[\|\|\phi(G(x)) - \phi(x)\|\|_1]$	This loss is to ensure that the resulting data achieved from generator G retains the same content as the input. $\phi(\cdot)$ represents feature maps, and it adopts an l_1 distance to measure the cross-quality content loss.
L_{prec}	$E_{x,y}[\|\|V(y) - V(G(x))\|\|_1]$	The perceptual loss is to ensure that the resulting data achieved from generator G retains the same content as the output. $V(\cdot)$ represents feature maps, and it adopts an l_1 distance to measure the cross-quality content loss. Incorporating a perceptual loss during network training can yield visually more realistic results.
L_{text}	$\sum_l \|\|T_l(\phi(F(\hat{I}^L))) - T_l(\phi(I^H))\|\|_2^2$	A texture descriptor [93], involving several Gram matrices T_l.
L_{cyc}	$E_{x \sim A}[\|\|G_B(G_A(x)) - x\|\|_1] +$ $E_{y \sim B}[\|\|G_A(G_B(y)) - y\|\|_1]$	Enforce forward-backward transformation consistency.
L_{seg}	$-\sum_i \log(Seg(G_1(x_i)))$	The segmentation loss is the weighted cross entropy loss. $Seg(\cdot)$ is the segmentation network.
L_{seg1}	$E_{x,c}[S(G(x,c), gt]$	We concatenate the corresponding modality label c to the synthesized image as the input of the segmentation network S. gt is the ground truth of the tumor segmentation map.
L_{iden}	$E_{y \sim B}[\|\|G_Y(y) - y\|\|_1]$	Identity consistency constraint, which can regularize the generator to preserve the colors and intensities during translation.
L_{rec1}	$E_{x \sim A, y \sim B, z \sim P(z)}\|\|y - G(x,z)\|\|_1$	The image y is reconstructed by generator G using the input x with the l_1 constraint. $P(z)$ is the standard normal distribution and $z \sim P(z)$ is the sampled latent vector.
L_{rec2}	$E_{x \sim A, y \sim B, z \sim P(z)}\|\|y - G(x,z)\|\|_2$	Similar with L_{rec} but uses l_2 constrain.
L_{kl}	$\mathbb{E}[D_{KL}(E(y))\|\|N(0,1)]$	To ensure the encoded vector has a similar distribution to the sampled latent vector, the KL-divergence constraint is enforced in the encoder network. It means that the difference between the encoded vector and the latent vector should be minimized. $\mathbb{E}$ denotes the expected value, E represents the encoder, D_{KL} denotes KL divergence, and z represents the latent vector sampled from the standard normal space.
L_{cla}	$L_{CE}(C(E(G(I_i, c_i), c_i), c_j), c_j) +$ $L_{CE}(C(E(I_i, c_i), c_i))$	Contrast-classification loss is to force classifier C to predict the contrast of extracted features by encoder E. We adversarially train the classifier to make deep features of multiple contrasts extracted by E to be same distributed, i.e., within a common feature space, using a gradient reversal layer in C, which flips gradient sign during backpropagation to force extracted deep features unable to be classified by C. L_{CE} computes the cross entropy between estimated contrast probability by C and real contrast code.
L_{cls}	$-y \log(x) - (1-y) \log(1-p(x))$	Universal cross-entropy loss. $p(x)$ is the estimated probability of x belonging to the correct class y.
L_{am}	$E_{p_a(x)}[\|\|(\mathbf{1} - M_x) \odot (G(x^a) - x^a)\|\|_2^2]$	For this medical imaging task in which accuracy is a major requirement of the model, the generator G needs to detect and modify the lesion region while keeping other parts unchanged. The L_{am} penalty is meant to enforce this, but to further help in this task we include a global shortcut to require the generator to learn a mapping that isolates and removes the lesion. M_x is mask of x. $\odot$ represents element-wise multiplication and $\mathbf{1}$ is an all-ones matrix of the same size as the input image.
L_{fm}	$\sum_k \sum_i \frac{1}{N_i} \|\|D_k^i(x,y) - D_k^i(x, G(x))\|\|_2^2$	Feature matching loss to stabilize training, which optimizes the generator to match these intermediate representations from the real and the synthesized images in multiple layers of the discriminators. D_k^i denotes the ith layer of the discriminator D_k, and N_i is the number of elements in the ith layer.
L_{sc}	$GDL(s, U(y)) + GDL(s, U(G(x)))$	Shape consistency loss is to regularize the generator to follow consistency relations. It adopts a generalized Dice loss (GDL) [90] to measure the difference between the predicted and real segmentation maps. $U(y)$ and $U(G(x))$ represent the predicted lesion segmentation probability maps by taking y and $G(x)$ as inputs in the segmentation module, respectively. s denotes the ground truth lesion segmentation map.
L_{cm}	$c \otimes \|\|\hat{y} - y\|\|_1 - \lambda \sum_i \sum \log(c^{ij})$	Confident map loss is to model the data-dependent aleatoric uncertainty. $\hat{y}$ is intermediate synthesis results of synthesized image y. c is the confidence map. To avoid a trivial solution (i.e. $c^{ij} = 0, \forall i, j$), λ is a constant adjusting the weight of this regularization term.

Hence, it is an urgent issue that there is not enough data to support the research for cross-modality synthesis except for MRI-to-MRI synthesis. In addition, according to Fig. 4, the publicly available MRI datasets are quite small. The largest dataset, BraTS [9], only contains 3000 subjects. Most MRI-to-MRI datasets contain no more than 500 subjects. Moreover, we can find that a lot of public MRI-to-MRI datasets have no ground truths for downstream tasks, like segmentation and classification. Since cross-modality synthesis aims to serve the downstream task, it is not easy to evaluate the real value of the synthesized neuroimage without the label for the downstream task. Most evaluation metrics, like PSNR and SSIM, are proposed to measure the quality of natural images, which cannot reflect the quality of cross-modality neuroimages. Thus, the performance of downstream tasks is a more robust metric for cross-modality neuroimage synthesis [42].

Table 6. A brief summary of different losses for cross-modality neuroimage synthesis (continuation of Table 5)

Abbr.	Function	Description
L_{dice}	$1 - \frac{1}{L}\sum_{l=1}^{L}\frac{\sum_p 2\hat{y}_p y_p(l)}{\hat{y}_p(l)^2 + \sum_p y_p(l)^2}$	Dice loss [71] measures the segmentation accuracy, where L is the total number of classes, p is the spatial position index in the image, $\hat{y}(l)$ is the predicted segmentation probability map for class l from the segmentation network and $y(l)$ is the ground truth segmentation mask for class l.
L_{reg}	$E_{x \sim \mathcal{X}}\left[\left\|\mathcal{A}_{\mathcal{X}}(x)\mathcal{A}_{\mathcal{X}}(x)^T - 1\right\|_F\right] +$ $E_{y \sim}\left[\left\|\mathcal{A}_{\mathcal{X}}(G_{\mathcal{X}}(y))\mathcal{A}_{\mathcal{X}}(G_{\mathcal{X}}(y))^T - 1\right\|\right]_F$	Attention regularization loss term encourages the attention maps to be orthogonal to each other. $\mathcal{A}$ the attention module. 1 is the identity matrix and $\|\cdot\|_F$ denotes the Frobenius norm.
L_{liu}	$\frac{1}{n}\sum_{i=i}^{n}\frac{\sigma(p_i)}{\mu(p_i)} + \frac{1}{n}\sum_{i=i}^{n}\frac{\sigma(q_i)}{\mu(q_i)}$	To well handle the spatiotemporally-heterogeneous intensity changes of the brain MR images, L_{liu} is designed to encourage the local intensity homogeneity in the corrected image. We assume that, for each brain tissue, i.e., gray matter (GM) and white matter (WM), the intensity values of the corrected image within a local patch are relatively homogeneous. p_i and q_j denote the ith and jth local patches sampled from the GM and WM of the "corrected" image, respectively. The operators $\sigma(\cdot)$ and $\mu(\cdot)$ are the standard deviation and mean, respectively. $\sigma(\cdot)/\mu(\cdot)$ calculates the coefficient of variation for a local patch.
L_{cor}	$\gamma(1 - \kappa_\zeta(G(v), f))$	L_{cor} can more sensitively suppress the negative influence from the outliers or impulsive noises, and thus help stabilize the training procedure and consequently improve the quality of the bias fields. $\kappa_\zeta(G(v), f) = \exp(-\frac{(G(v)-f)^2}{2\zeta^2})$ is the Gaussian kernel, ζ is the corresponding tuning bandwidth, and $\gamma = (1 - \exp(-\frac{1}{2\zeta^2}))^{-1}$.
L_{sm}	$\|\Delta G(v)\|_2^2$	The bias fields $G(v)$ estimated from the input intensity images should be smooth. A smoothness loss function is based on the Laplacian operator to provide explicit guidance of the smoothness constraint.
L_{ssim}	$-\log(\frac{1}{2|P|}\sum_{p \in P}(1 + SSIM(p)))$	Structural similarity index loss. P denotes the set of pixel location and $|P|$ is its cardinality. $SSIM(\cdot)$ is one of the perceptual metrics and it is also differentiable.
L_{mc}	$E_{\sim \hat{x}_y}[-\log(D(\hat{x}_y, m_y))] +$ $E_{\sim x}[-\log(D(x, m_x))]$	Modality classification loss. Given the pair of input sample and target modality x, m_y, we propose to learn a parameterized mapping $f : x, m_y \rightarrow \hat{x}_y$ from x, m_y to the generated corresponding sample with modality my to closely resemble x_y. m_y denotes a four-dimensional one-hot vector to represent the four MR modalities
L_{gdl}	Gradient difference loss	To deal with the inherent blurry effect.
L_{edge}	Edge-aware constraint	Based on the similarity of the edge maps from synthesized and real images.
L_{tumor}	Tumor-aware constraint	The edge-aware learning helps the model capture the context information of the entire brain, but not necessarily for individual tumors. Since tumor appearance is highly variable and subject-specific, it is hard to synthesize than the normal tissue.
L_{mani}	Manifold regularizer	To preserve the complementary properties. Since the image manifold reflects the intrinsic geometric structure underlying the data leading to the generated results with a realistic overall structure.
L_{mmd}	Regularization	Maximum mean discrepancy regularization [22].
L_{gcr}	Regularization	Geometry co-regularization.
L_{ae}	Reconstruction	Autoencoder reconstruction.
L_{oth}	Regularization	Spectral restricted isometry property regularization [5].
L_{fault}	Fault-aware discriminator	To make the synthesized results can satisfy the requirement of segmentation and substitute the real acquisitions in practice, and bridge the gap of segmentation performance between synthesized data and real ones.

4.2 Losses

Table 5 and Table 6 provide a comprehensive overview of the loss functions in cross-modality neuroimage synthesis. The second column in Table 5 and Table 6 denotes the loss function. The third column describes the details or the role of the loss function. We categorize the overall loss functions into three streams. The first category is the basic class of GAN loss functions, including the adversarial loss function L_{gan} and its variants L_{sgan} and L_{cgan}, the cycle loss function L_{cyc}, the pixel identity loss function L_{p2p}, the edge identity loss function L_{edge}. They are commonly used for the general cross-modality synthesis but are not specifically designed for cross-modality neuroimage synthesis. The second category of loss functions is the regularizer loss function. They construct the optimization problems by utilizing the intrinsic characteristic of neuroimaging. For instance, L_{mmd} is the maximum discrepancy regularization when seeking the paired feature points from the source and target modality neuroimage. L_{cor} stabilizes the training procedure and improves the bias field quality by suppressing the negative influence from the outlier noise. L_{tumor} utilizes the similarity contextual information for both T1 and T2 modalities to regularize the quality of synthesized neuroimage. L_{sc} regularizes the generator to ensure adherence to the consistency of tumor shape among multi-modalities neuroimages. The third category of loss functions is strongly related to the downstream task, like segmentation loss L_{seg}, dice score loss L_{dice}, cross-entropy loss L_{cls}, and modality classification loss L_{mc}. These loss functions aim to optimize the downstream task with cross-modality neuroimage synthesis jointly.

Table 7. A brief summary of different metrics for cross-modality neuroimage synthesis.

Acronyms	Level	Name	Description
PSNR	↑	Peak signal-to-noise ratio	
SSIM	↑	Structural similarity	
MSSSIM	↑	Multiscale structural similarity	
MAE	↓	Mean absolute error	
DSC	↑	Dice similarity coefficient	DSC is employed to evaluate different approaches by comparing their segmentation results against the ground truth voxel-by-voxel.
ASD/ASSD	↑	Average (symmetric) surface distance	It is used to compute the average surface distance from y_{pred} to y under the default setting. This tells us how much, on average, the segmentation surface deviates from the GT.
MOS	↑	Mean opinion score	Measure the quality of a given image by a rating score between 1 and 5: 1 indicates inferior while 5 indicates superior.
DS	↓	Deformation score	A registration metric based on Jacobian. For DS, an FFD-based [83] deformable registration is applied to the synthesised MR to register it to a real MR at a similar imaging plane. The average Jacobian (normalised to [0,1)) of the required deformation to complete such registration was computed as the score consequently. The underlying assumption is that a synthesised MRI with high quality tends to have a lower Jacobian when registering to the real MRI.
P	↑	Precision	The fraction of true positive examples among the examples that the model classified as positive.
R	↑	Recall	The fraction of examples classified as positive, among the total number of positive examples.
F1S	↑	F1 score for classification	It is defined as $2(P \times R)/(P + R)$.
F-score	↑	F1 score for segmentation	Measure the overlap of ground truth segmentation labels. It is defined as $(2|H \cap G|)/(|H| + |G|)$ where G is the label of the target image and H is the prediction of the source image.
VS	↑	Verisimilitude score	A higher VS means more produced pseudo-healthy images fool the classifier successfully, indicating the model can better generate lesion-free images lying in the true data distribution of normal images.
MSE	↓	Mean-squared error	
NMSE	↓	Normalized mean-squared error	
RMSE	↓	Root mean-squared error	
NRMSE	↓	Normalized root mean-squared error	
HD95	↓	95th Hausdorff Distance	
CC	↓	Correlation coefficient	
CIV	↑	Coefficient of intensity variation	
L1	↓	L1 error	
L2	↓	L2 error	
t-L2	↓	Tumor-averaged L2	Based on segmentation maps of enhancing lesions.
FID	↓	Fréchet inception distance	For the evaluation of the performance of synthesis models at image generation [30].
UQI	↑	Universal quality index	This index is designed by modeling any image distortion as a combination of three factors: loss of correlation, luminance distortion, and contrast distortion [103].
MMD	↓	Maximum mean discrepancy	
IS	↑	Inception score	
ACC	↑	Accuracy	
AUC	↑	Area under curve	Area under the receiver operating characteristic.
ROC	↑	Receiver operator characteristic	Show the diagnostic ability of binary classifiers.
BAC	↑	Balanced accuracy	
SEN	↑	Sensitivity	
SPE	↑	Specificity	
MCC	↑	Matthews correlation coefficient	[68]
DVR	↑	[^{11}C]PIB PET distribution volume ratio	Relect the myelin content.
MI	↑	Mutual information	[104]
Q	↑	Weighted fusion quality metric	[78]
FMI	↑	Feature mutual information measures	[24]

4.3 Metrics

Table 7 provides a comprehensive review of the metrics in cross-modality neuroimage synthesis. The first and third columns list the acronym and full name of a metric, respectively. The up arrow in the second column indicates that a higher value represents a better result; the opposite applies for the down arrow. The last column provides additional descriptions, which are tailored for cross-modality neuroimage synthesis if possible. From Table 7, it can be easily observed that most of the novel metrics are variants of traditional metrics, such as MAE, PSNR, or SSIM. The traditional

metrics are fast to compute; however, they cannot reflect the true quality of neuroimage because they focus more on the low-level pixel-wise fidelity and ignore the fundamental traits of neuroimages, such as the structural characteristics of the lesion area and the k-space feature drift. One alternative approach to alleviate this problem is to use downstream tasks such as segmentation or classification to validate the quality of generated samples [39, 40]. Nevertheless, The drawbacks associated with this approach are as follows. 1) The computational expense is substantial, often necessitating the utilization of GPUs for computation. 2) The additional segmentation significantly influences the inference speed. 3) This approach cannot be seamlessly integrated into an end-to-end optimization for cross-modality neuroimage synthesis. Hiring a radiologist for review is another option, but it is too costly, time-consuming, and difficult to scale up. Hence, the validity of these metrics for neuroimages remains to be explored.

5 OPEN CHALLENGES AND FUTURE DIRECTIONS

As an emerging area, research on multi-modality brain image synthesis is still in its infancy. The remaining challenging topics and potential solutions are summarized as follows.

Challenge 1: Joint optimization of the synthesis model and downstream task. How to jointly optimize the cross-modality neuroimage synthesis and the downstream tasks with either weakly supervised or unsupervised learning? Previously, neuroimage synthesis [44, 87] is generally regarded as a standalone task, which overlooks one crucial fact, namely whether the synthesized results can improve the downstream tasks.

Solution 1: Multi-task learning. Transforming downstream tasks and cross-modality synthesis into multi-task learning improves both the quality of synthesized neuroimages and the performance of downstream tasks. Recently, there are some initial attempts in the joint optimization of cross-modality neuroimage synthesis and downstream tasks. Unsupervised learning methods [26, 91, 118] and weakly supervised learning approaches [86, 129] start paying attention to downstream tasks rather than focusing only on the quality of the synthesized results.

Challenge 2: Correctness of synthesized lesions. How to ensure the correctness of the synthesized lesions? Previously, most cross-modality image synthesis algorithms pay attention to the quality of the whole image, which fail to highlight the essential regions related to disease (see Fig. 3).

Solution 2: Lesion-oriented synthesis. The method reported in [91] provides a potential answer to this question since the diagnosis of the lesion can be treated as an anomaly detection task. If we can detect the disease region and use it as guidance for cross-modality brain image synthesis, the generated output is steered in a disease-highlighted and lesion-oriented manner.

Challenge 3: Dedicated evaluation metrics. How to identify an appropriate metric to evaluate the results of cross-modality image synthesis? Existing measurements are usually based on the PSNR and SSIM, which are established on natural images but ignore the inherent properties of neuroimages. The translated medical data with the highest PSNR or SSIM may still be blurred, or miss important neural tissue representations.

Solution 3: K-space-aware metrics. The concept of k-space imaging is the main distinction between MR imaging and natural images, in addition to the disease area. The new synthetic quality metric should accurately reflect the location of the critical lesion and the essential k-space characteristics of neuroimages. Therefore, the new metric should encompass the lesion region, k-space characteristics, and anatomical features.

Challenge 4: Misaligned data usage. How to utilize misaligned or unpaired neuroimaging data for cross-modality image synthesis? In practice, a large amount of misaligned neuroimaging data exists in each vendor (i.e., hospital). The state-of-the-art image registration algorithm takes a lot of time to register a pair of brain images, especially across modalities. It also requires a great deal of laborious work to verify the registration result, and correct residual

errors if necessary. Whether the strong dependence on registration can be eliminated for cross-modality synthesis is questionable.

Solution 4: Misaligned neuroimage as data augmentation. Kong *et al.* [54] and Wang *et al.* [98] attempt to eliminate the need for registration and make full use of misaligned neuroimaging data for synthesis. The work of [54] incorporates the correction loss into CycleGAN [132], while Wang *et al.* [98] regard the misaligned neuroimaging data as a data augmentation of the self-supervised learning method and design an affined transformation loss to enable the discriminator overcoming the over-fitting problem. Furthermore, the authors in [98] stimulate severely misaligned neuroimaging data and find that their methods perform better in the presence of severe misalignment.

Challenge 5: A unified model. How to build up a unified model for cross-modality brain image synthesis?

Solution 5: One to many via invariant features. Previously, most works focused on modality synthesis in MR, CT, and PET. Charts *et al.* [9] propose a multi-input and multi-output fully convolutional network model to synthesize various modalities of MRI. Similarly to the work of [9], Liu *et al.* [62] propose a unified conditional disentanglement work to synthesize various modalities of MRI. Moreover, in order to speed up the inference phase, Zhang *et al.* [124] provides an excellent way to speed up the modal-specific feature retrieval by transferring knowledge from original data to hash codes. However, simultaneous synthesis of varying MR, CT, and PET modalities is lacking. The work of [130] may provide a solution, which uses a cycle-consistent GAN to extract the invariant features from various modalities. Nevertheless, its synthesis mode is limited in MRI-to-MRI. The invariant characteristics from CT, PET, and MRI should be extracted to train a unified synthesis model in the future.

Challenge 6: Data privacy. How can the data isolation problems be solved while protecting the patients' privacy for cross-modality brain image synthesis? The current state-of-the-art brain image synthesis algorithms consider a centralized training strategy. However, many medical institutions cannot share their data, which is restricted by privacy protection legislation.

Solution 6: Federated cross-modality neuroimage synthesis. Wang *et al.* [97] are the first to address this issue. They find out that the clipped gradient enhances the data privacy guarantee and increases the fidelity of synthesized neuroimages. Then FedMed-ATL [98] presents a more unbalanced data setting for clients to simulate the more realistic scenario.

6 FUTURE PRACTICAL APPLICATIONS

There are two scenarios in which cross-modality neuroimage synthesis can be applied. First and foremost, as mentioned in **Challenge 1** of Section 5, cross-modality neuroimage synthesis serves as an auxiliary method for diagnosis, such as investigating pathology and neurodegeneration [77]. Therefore, it is necessary to ensure that the synthesized neuroimage is optimized to improve the performance of downstream tasks, such as tumor detection [26, 91, 118] and segmentation [86]. To achieve this goal, utilizing multi-task learning to simultaneously optimize the synthesis of neuroimages across different modalities and their downstream tasks is an up-and-coming area of research. Second, as discussed in **Challenge 4** of Section 5, using cross-modality neuroimage synthesis to minimize the manual effort required for registration is an additional area of great potential. Previously, the registration process for misaligned neuroimages required a significant amount of manual effort [4, 53], leading to low throughput in practice. Registration-free cross-modality neuroimage synthesis gains attraction in academia [13, 54], which can dramatically reduce physicians' workload. However, physicians still need to verify the content generated, and further future exploration of its interpretability is required. Third, as mentioned in **Challenge 5** of Section 5, there is a scarcity of cross-modality neuroimage synthesis models that can simultaneously synthesize MR, CT, and PET. Deploying multi-synthesis models

in medical institutions is impractical due to limited storage capacity. Therefore, developing a cohesive cross-modality neuroimage synthesis model within the medical imaging community is imperative. Finally, as presented **Challenge 6** of Section 5, data privacy remains a significant concern in the field of cross-modality neuroimage synthesis. Training a cross-modality neuroimage synthesis model often requires a large number of neuroimages. However, collecting a large number of neuroimages for training is challenging due to privacy regulations. Hence, incorporating federated learning into cross-modality neuroimage synthesis holds great potential in effectively leveraging a multitude of neuroimages from different medical institutions while adhering to privacy regulations.

7 CONCLUSION

In this paper, we provided a literature review on cross-modality brain image synthesis, focusing on the level of supervision, downstream tasks, modalities, datasets, loss functions, and evaluation metrics. In particular, we characterized the architecture of existing cross-modality synthesis models based on the supervision level. In addition, for each downstream task, we analyzed in detail how cross-modality neuroimage synthesis enhances its performance. In the end, we highlighted a number of exciting future research directions for cross-modality neuroimage synthesis. In conclusion, the recent prevalence of cross-modality neuroimage synthesis significantly impacted downstream tasks in the medical imaging field. However, multi-task learning with cross-modality neuroimage synthesis and other downstream tasks were still in the early research phase. We hope the review and analysis presented in this paper will inspire researchers to develop more effective cross-modality neuroimage synthesis methods for practical applications.

ACKNOWLEDGMENTS

REFERENCES

[1] Michal Aharon, Michael Elad, and Alfred Bruckstein. 2006. K-SVD: An algorithm for designing overcomplete dictionaries for sparse representation. *IEEE Transactions on Signal Processing* 54, 11, 4311–4322.

[2] Omar S Al-Kadi, Israa Almallahi, Alaa Abu-Srhan, AM Mohammad Abushariah, and Waleed Mahafza. 2022. Unpaired MR-CT brain dataset for unsupervised image translation. *Data in Brief* 42 (2022), 108109.

[3] Paul Aljabar, Robin Wolz, Latha Srinivasan, Serena J. Counsell, Mary A. Rutherford, Anthony David Edwards, Joseph V. Hajnal, and Daniel Rueckert. 2011. A combined manifold learning analysis of shape and appearance to characterize neonatal brain development. *IEEE Transactions on Medical Imaging* 30 (2011), 2072–2086.

[4] Brian B Avants, Nicholas J Tustison, Gang Song, Philip A Cook, Arno Klein, and James C Gee. 2011. A reproducible evaluation of ANTs similarity metric performance in brain image registration. *Neuroimage* 54, 3 (2011), 2033–2044.

[5] Nitin Bansal, Xiaohan Chen, and Zhangyang Wang. 2018. Can we gain more from orthogonality regularizations in training deep networks? *Advances in Neural Information Processing Systems* 31 (2018).

[6] Xuesheng Bian, Xiongbiao Luo, Cheng Wang, Weiquan Liu, and Xiuhong Lin. 2022. DDA-Net: Unsupervised cross-modality medical image segmentation via dual domain adaptation. *Computer Methods and Programs in Biomedicine* 213 (2022), 106531.

[7] Alexandre Bône, Samy Ammari, Jean-Philippe Lamarque, Mickael Elhaik, Émilie Chouzenoux, François Nicolas, Philippe Robert, Corinne Balleyguier, Nathalie Lassau, and Marc-Michel Rohé. 2021. Contrast-enhanced brain MRI synthesis with deep learning: key input modalities and asymptotic performance. *IEEE 18th International Symposium on Biomedical Imaging* (2021), 1159–1163.

[8] Agisilaos Chartsias, Thomas Joyce, Mario Valerio Giuffrida, and Sotirios A Tsaftaris. 2017. Multimodal MR synthesis via modality-invariant latent representation. *IEEE Transactions on Medical Imaging* 37, 3 (2017), 803–814.

[9] Agisilaos Chartsias, Thomas Joyce, Mario Valerio Giuffrida, and Sotirios A. Tsaftaris. 2018. Multimodal MR synthesis via modality-invariant latent representation. *IEEE Transactions on Medical Imaging* 37 (2018), 803–814.

[10] Cheng Chen, Qi Dou, Hao Chen, and Pheng-Ann Heng. 2018. Semantic-aware generative adversarial nets for unsupervised domain adaptation in Chest X-ray segmentation. *International Conference on Medical Image Computing and Computer-Assisted Intervention.*

[11] Cheng Chen, Qi Dou, Hao Chen, Jing Qin, and Pheng-Ann Heng. 2020. Unsupervised bidirectional cross-modality adaptation via deeply synergistic image and feature alignment for medical image segmentation. *IEEE Transactions on Medical Imaging* 39 (2020), 2494–2505.

[12] Liangjun Chen, Zhengwang Wu, Dan Hu, Fan Wang, J. Keith Smith, Weili Lin, Li Wang, Dinggang Shen, and Gang Li. 2021. ABCnet: Adversarial bias correction network for infant brain MR images. *Medical Image Analysis* 72 (2021), 102133.

[13] Runfa Chen, Wenbing Huang, Binghui Huang, Fuchun Sun, and Bin Fang. 2020. Reusing discriminators for encoding: Towards unsupervised image-to-image translation. *Proceedings of the IEEE/CVF Conference on Computer Vision and Pattern Recognition*, 8168–8177.

[14] Zekang Chen, Jia Wei, and Rui Li. 2022. Unsupervised multi-modal medical image registration via discriminator-free image-to-image translation. *International Joint Conferences on Artificial Intelligence.*

[15] Hong Cheng, Zicheng Liu, Lu Yang, and Xuewen Chen. 2013. Sparse representation and learning in visual recognition: theory and applications. *Signal Processing* 93, 6 (2013), 1408–1425.

[16] Salman Ul Hassan Dar, Mahmut Yurt, Levent Karacan, Aykut Erdem, Erkut Erdem, and Tolga Çukur. 2019. Image synthesis in multi-contrast MRI with conditional generative adversarial networks. *IEEE Transactions on Medical Imaging* 38 (2019), 2375–2388.

[17] Michael Elad. 2012. Sparse and redundant representation modeling—What next? *IEEE Signal Processing Letters* 19, 12 (2012), 922–928.

[18] Kathryn A Ellis, Ashley I Bush, David Darby, Daniela De Fazio, Jonathan Foster, Peter Hudson, Nicola T Lautenschlager, Nat Lenzo, Ralph N Martins, Paul Maruff, et al. 2009. The Australian Imaging, Biomarkers and Lifestyle (AIBL) study of aging: methodology and baseline characteristics of 1112 individuals recruited for a longitudinal study of Alzheimer's disease. *International Psychogeriatrics* 21, 4 (2009), 672–687.

[19] Ying Fu, Antony Lam, Imari Sato, and Yoichi Sato. 2015. Adaptive spatial-spectral dictionary learning for hyperspectral image denoising. *Proceedings of the IEEE/CVF International Conference on Computer Vision*, 343–351.

[20] Shenghua Gao, Ivor Wai-Hung Tsang, and Liang-Tien Chia. 2012. Laplacian sparse coding, hypergraph laplacian sparse coding, and applications. *IEEE Transactions on Pattern Analysis and Machine Intelligence* 35, 1 (2012), 92–104.

[21] Raja Giryes and Michael Elad. 2014. Sparsity-based poisson denoising with dictionary learning. *IEEE Transactions on Image Processing* 23, 12 (2014), 5057–5069.

[22] Arthur Gretton, Karsten M Borgwardt, Malte J Rasch, Bernhard Schölkopf, and Alexander Smola. 2012. A kernel two-sample test. *The Journal of Machine Learning Research* 13, 1 (2012), 723–773.

[23] Pengfei Guo, Puyang Wang, Rajeev Yasarla, Jinyuan Zhou, Vishal M. Patel, and Shanshan Jiang. 2021. Anatomic and molecular MR image synthesis using cnfidence guided CNNs. *IEEE Transactions on Medical Imaging* 40 (2021), 2832–2844.

[24] Mohammad Haghighat and Masoud Amirkabiri Razian. 2014. Fast-FMI: Non-reference image fusion metric. *IEEE 8th International Conference on Application of Information and Communication Technologies (AICT)*, 1–3.

[25] Xiao Han. 2017. MR-based synthetic CT generation using a deep convolutional neural network method. *Medical Physics* 44 (2017), 1408–1419.

[26] Yufan He, Aaron Carass, Lianrui Zuo, Blake E. Dewey, and Jerry L Prince. 2021. Autoencoder based self-supervised test-time adaptation for medical image analysis. *Medical Image Analysis* 72 (2021), 102136.

[27] Yuan He, Aoyu Wang, Shuai Li, Yikang Yang, and Aimin Hao. 2022. Nonfinite-modality data augmentation for brain image registration. *Computers in Biology and Medicine* 147 (2022), 105780.

[28] Rolf A. Heckemann, Joseph V. Hajnal, Paul Aljabar, Daniel Rueckert, and Alexander Hammers. 2006. Automatic anatomical brain MRI segmentation combining label propagation and decision fusion. *Neuroimage* 33 (2006), 115–126.

[29] Matt Hemsley, Brige P. Chugh, Mark Ruschin, Young Lee, Chia-Lin Tseng, Greg J. Stanisz, and Angus Z. Lau. 2020. Deep generative model for synthetic-CT generation with uncertainty predictions. *International Conference on Medical Image Computing and Computer-Assisted Intervention.*

[30] Martin Heusel, Hubert Ramsauer, Thomas Unterthiner, Bernhard Nessler, and Sepp Hochreiter. 2017. Gans trained by a two time-scale update rule converge to a local nash equilibrium. *Advances in Neural Information Processing Systems* 30 (2017).

[31] Yuta Hiasa, Yoshito Otake, Masaki Takao, Takumi Matsuoka, Kazuma Takashima, Jerry L Prince, Nobuhiko Sugano, and Yoshinobu Sato. 2018. Cross-modality image synthesis from unpaired data using CycleGAN: Effects of gradient consistency loss and training data size. *ArXiv* abs/1803.06629 (2018).

[32] Brittany R Howell, Martin A Styner, Wei Gao, Pew-Thian Yap, Li Wang, Kristine Baluyot, Essa Yacoub, Geng Chen, Taylor Potts, Andrew Salzwedel, et al. 2019. The UNC/UMN Baby Connectome Project (BCP): An overview of the study design and protocol development. *Neuroimage* 185 (2019), 891–905.

[33] Shengye Hu, Baiying Lei, Shuqiang Wang, Yong Wang, Zhiguang Feng, and Yanyan Shen. 2022. Bidirectional mapping generative adversarial networks for brain MR to PET synthesis. *IEEE Transactions on Medical Imaging* 41 (2022), 145–157.

[34] Shengye Hu, Yanyan Shen, Shuqiang Wang, and Baiying Lei. 2020. Brain MR to PET synthesis via bidirectional generative adversarial network. *International Conference on Medical Image Computing and Computer-Assisted Intervention.*

[35] De-An Huang and Yu-Chiang Frank Wang. 2013. Coupled dictionary and feature space learning with applications to cross-domain image synthesis and recognition. *Proceedings of the IEEE/CVF International Conference on Computer Vision*, 2496–2503.

[36] Pu Huang, Dengwang Li, Zhicheng Jiao, Dongming Wei, Guoshi Li, Qian Wang, Han Zhang, and Dinggang Shen. 2019. CoCa-GAN: Common-feature-learning-based context-aware generative adversarial network for glioma grading. *International Conference on Medical Image Computing and Computer-Assisted Intervention.*

[37] Yawen Huang, Leandro Beltrachini, Ling Shao, and Alejandro F Frangi. 2016. Geometry regularized joint dictionary learning for cross-modality image synthesis in magnetic resonance imaging. *International Conference on Medical Image Computing and Computer-Assisted Intervention.*

[38] Yawen Huang, Ling Shao, and Alejandro F. Frangi. 2017. DOTE: dual convolutional filter learning for super-resolution and cross-modality synthesis in MRI. *International Conference on Medical Image Computing and Computer-Assisted Intervention.*

[39] Yawen Huang, Ling Shao, and Alejandro F. Frangi. 2017. Simultaneous super-resolution and cross-modality synthesis of 3D medical images using weakly-supervised joint convolutional sparse coding. *Proceedings of the IEEE/CVF Conference on Computer Vision and Pattern Recognition* (2017), 5787–5796.

[40] Yawen Huang, Ling Shao, and Alejandro F. Frangi. 2018. Cross-Modality image synthesis via weakly coupled and geometry co-regularized joint dictionary learning. *IEEE Transactions on Medical Imaging* 37 (2018), 815–827.

[41] Yawen Huang, Ling Shao, and Alejandro F. Frangi. 2019. Simultaneous super-resolution and cross-modality synthesis in magnetic resonance imaging. *Deep Learning and Convolutional Neural Networks for Medical Imaging and Clinical Informatics.*

[42] Yawen Huang, Feng Zheng, Runmin Cong, Weilin Huang, Matthew R. Scott, and Ling Shao. 2020. MCMT-GAN: multi-task coherent modality transferable GAN for 3D brain image synthesis. *IEEE Transactions on Image Processing* 29 (2020), 8187–8198.

[43] Yawen Huang, Feng Zheng, Danyang Wang, Junyu Jiang, Xiaoqian Wang, and Ling Shao. 2020. Super-resolution and inpainting with degraded and upgraded generative adversarial networks. *International Conference on Medical Image Computing and Computer-Assisted Intervention.*

[44] Yuankai Huo, Zhoubing Xu, Hyeonsoo Moon, Shunxing Bao, Albert Assad, Tamara K. Moyo, Michael R. Savona, Richard G. Abramson, and Bennett A. Landman. 2019. SynSeg-Net: Synthetic segmentation without target modality ground truth. *IEEE Transactions on Medical Imaging* 38 (2019), 1016–1025.

[45] Tri Huynh, Yaozong Gao, Jiayin Kang, Li Wang, Pei Zhang, Jun Lian, and Dinggang Shen. 2015. Estimating CT image from MRI data using structured random forest and auto-context model. *IEEE Transactions on Medical Imaging* 35, 1 (2015), 174–183.

[46] Phillip Isola, Jun-Yan Zhu, Tinghui Zhou, and Alexei A. Efros. 2017. Image-to-image translation with conditional adversarial networks. *Proceedings of the IEEE/CVF Conference on Computer Vision and Pattern Recognition* (2017), 5967–5976.

[47] Clifford R Jack Jr, Matt A Bernstein, Nick C Fox, Paul Thompson, Gene Alexander, Danielle Harvey, Bret Borowski, Paula J Britson, Jennifer L. Whitwell, Chadwick Ward, et al. 2008. The Alzheimer's disease neuroimaging initiative (ADNI): MRI methods. *Journal of Magnetic Resonance Imaging: An Official Journal of the International Society for Magnetic Resonance in Medicine* 27, 4 (2008), 685–691.

[48] Jianbo Jiao, Ana I. L. Namburete, Aris T. Papageorghiou, and Julia Alison Noble. 2020. Self-supervised ultrasound to MRI fetal brain image synthesis. *IEEE Transactions on Medical Imaging* 39 (2020), 4413–4424.

[49] Amod Jog, Aaron Carass, Snehashis Roy, Dzung L. Pham, and Jerry L Prince. 2017. Random forest regression for magnetic resonance image synthesis. *Medical Image Analysis* 35 (2017), 475–488.

[50] Thomas Joyce, Agisilaos Chartsias, and Sotirios A. Tsaftaris. 2017. Robust multi-modal MR image synthesis. *International Conference on Medical Image Computing and Computer-Assisted Intervention.*

[51] Chia-Hsiang Kao, Yong-Sheng Chen, Li-Fen Chen, and Wei-Chen Chiu. 2021. Demystifying T1-MRI to FDG[18] -PET image translation via representational similarity. *International Conference on Medical Image Computing and Computer-Assisted Intervention*, 402–412.

[52] Kerstin Kläser, Thomas Varsavsky, Pawel J. Markiewicz, Tom Kamiel Magda Vercauteren, Alexander Hammers, David Atkinson, K. Thielemans, Brian F. Hutton, Manuel Jorge Cardoso, and Sébastien Ourselin. 2021. Imitation learning for improved 3D PET/MR attenuation correction. *Medical Image Analysis* 71 (2021).

[53] Arno Klein, Jesper Andersson, Babak A Ardekani, John Ashburner, Brian Avants, Ming-Chang Chiang, Gary E Christensen, D Louis Collins, James Gee, Pierre Hellier, et al. 2009. Evaluation of 14 nonlinear deformation algorithms applied to human brain MRI registration. *Neuroimage* 46, 3 (2009), 786–802.

[54] Lingke Kong, Chenyu Lian, Detian Huang, Zhenjiang Li, Yanle Hu, and Qichao Zhou. 2021. Breaking the dilemma of medical image-to-image translation. *Advances in Neural Information Processing Systems* 34 (2021), 1964–1978.

[55] Gihyun Kwon, Chihye Han, and Dae-Shik Kim. 2019. Generation of 3D Brain MRI using auto-encoding generative adversarial networks. *International Conference on Medical Image Computing and Computer-Assisted Intervention.*

[56] Bennett A Landman, Alan J Huang, Aliya Gifford, Deepti S Vikram, Issel Anne L Lim, Jonathan AD Farrell, John A Bogovic, Jun Hua, Min Chen, Samson Jarso, et al. 2011. Multi-parametric neuroimaging reproducibility: a 3-T resource study. *Neuroimage* 54, 4 (2011), 2854–2866.

[57] Dongwook Lee, Junyoung Kim, Won-Jin Moon, and J. C. Ye. 2019. CollaGAN: Collaborative GAN for missing image data imputation. *Proceedings of the IEEE/CVF Conference on Computer Vision and Pattern Recognition* (2019), 2482–2491.

[58] Hongwei Li, Johannes C. Paetzold, Anjany Kumar Sekuboyina, Florian Kofler, Jianguo Zhang, Jan S. Kirschke, Benedikt Wiestler, and Bjoern H. Menze. 2019. DiamondGAN: unified multi-modal generative adversarial networks for MRI sequences synthesis. *ArXiv* abs/1904.12894 (2019).

[59] Zhengming Li, Zhihui Lai, Yong Xu, Jian Yang, and David Zhang. 2015. A locality-constrained and label embedding dictionary learning algorithm for image classification. *IEEE Transactions on Neural Networks and Learning Systems* 28, 2 (2015), 278–293.

[60] Sook-Lei Liew, Julia M Anglin, Nick W Banks, Matt Sondag, Kaori L Ito, Hosung Kim, Jennifer Chan, Joyce Ito, Connie Jung, Nima Khoshab, et al. 2018. A large, open source dataset of stroke anatomical brain images and manual lesion segmentations. *Scientific Data* 5, 1 (2018), 1–11.

[61] Geert Litjens, Oscar Debats, Jelle Barentsz, Nico Karssemeijer, and Henkjan Huisman. 2014. Computer-aided detection of prostate cancer in MRI. *IEEE Transactions on Medical Imaging* 33, 5 (2014), 1083–1092.

[62] Xiaofeng Liu, Fangxu Xing, Georges El Fakhri, and Jonghye Woo. 2021. A unified conditional disentanglement framework for multimodal brain Mr image translation. *IEEE 18th International Symposium on Biomedical Imaging* (2021), 10–14.

[63] Yunbi Liu, Ling Yue, Shifu Xiao, Wei Yang, Dinggang Shen, and Mingxia Liu. 2022. Assessing clinical progression from subjective cognitive decline to mild cognitive impairment with incomplete multi-modal neuroimages. *Medical Image Analysis* 75 (2022), 102266.

[64] Frederik Maes, André M. F. Collignon, Dirk Vandermeulen, Guy Marchal, and Paul Suetens. 1997. Multimodality image registration by maximization of mutual information. *IEEE Transactions on Medical Imaging* 16 (1997), 187–198.

[65] Oskar Maier, Bjoern H Menze, Janina von der Gablentz, Levin Häni, Mattias P Heinrich, Matthias Liebrand, Stefan Winzeck, Abdul Basit, Paul Bentley, Liang Chen, et al. 2017. ISLES 2015-A public evaluation benchmark for ischemic stroke lesion segmentation from multispectral MRI. *Medical Image Analysis* 35 (2017), 250–269.

[66] Julien Mairal, Francis Bach, Jean Ponce, et al. 2014. Sparse modeling for image and vision processing. *Foundations and Trends® in Computer Graphics and Vision* 8, 2-3 (2014), 85–283.

[67] M. Maspero, Mark Savenije, Anna M. Dinkla, Peter R. Seevinck, Martijn P W Intven, Ina M Jurgenliemk-Schulz, Linda G. W. Kerkmeijer, and Cornelis A. T. van den Berg. 2018. Dose evaluation of fast synthetic-CT generation using a generative adversarial network for general pelvis MR-only radiotherapy. *Physics in Medicine & Biology* 63 (2018).

[68] Brian W Matthews. 1975. Comparison of the predicted and observed secondary structure of T4 phage lysozyme. *Biochimica et Biophysica Acta (BBA)-Protein Structure* 405, 2 (1975), 442–451.

[69] Adriënne M Mendrik, Koen L Vincken, Hugo J Kuijf, Marcel Breeuwer, Willem H Bouvy, Jeroen De Bresser, Amir Alansary, Marleen De Bruijne, Aaron Carass, Ayman El-Baz, et al. 2015. MRBrainS challenge: online evaluation framework for brain image segmentation in 3T MRI scans. *Computational Intelligence and Neuroscience* 2015 (2015).

[70] Bjoern H Menze, Andras Jakab, Stefan Bauer, Jayashree Kalpathy-Cramer, Keyvan Farahani, Justin Kirby, Yuliya Burren, Nicole Porz, Johannes Slotboom, Roland Wiest, et al. 2014. The multimodal brain tumor image segmentation benchmark (BRATS). *IEEE Transactions on Medical Imaging* 34, 10 (2014), 1993–2024.

[71] Fausto Milletari, Nassir Navab, and Seyed-Ahmad Ahmadi. 2016. V-net: Fully convolutional neural networks for volumetric medical image segmentation. *The Fourth International Conference on 3D Vision (3DV)*, 565–571.

[72] Hien Van Nguyen, Shaohua Kevin Zhou, and Raviteja Vemulapalli. 2015. Cross-domain synthesis of medical images using efficient location-sensitive deep network. *International Conference on Medical Image Computing and Computer-Assisted Intervention*.

[73] Dong Nie, Roger Trullo, Caroline Petitjean, Su Ruan, and Dinggang Shen. 2017. Medical image synthesis with context-aware generative adversarial networks. *International Conference on Medical Image Computing and Computer-Assisted Intervention* 10435 (2017), 417–425.

[74] Sahin Olut, Yusuf Huseyin Sahin, Ugur Demir, and Gözde B. Ünal. 2018. Generative adversarial training for MRA image synthesis using multi-contrast MRI. *International Conference on Medical Image Computing and Computer-Assisted Intervention*.

[75] Yongsheng Pan, Mingxia Liu, Chunfeng Lian, Yong Xia, and Dinggang Shen. 2019. Disease-image specific generative adversarial network for brain disease diagnosis with incomplete multi-modal neuroimages. *International Conference on Medical Image Computing and Computer-Assisted Intervention*.

[76] Yongsheng Pan, Mingxia Liu, Chunfeng Lian, Tao Zhou, Yong Xia, and Dinggang Shen. 2018. Synthesizing missing PET from MRI with cycle-consistent generative adversarial networks for Alzheimer's disease diagnosis. *International Conference on Medical Image Computing and Computer-Assisted Intervention* 11072 (2018), 455–463.

[77] Yongsheng Pan, Mingxia Liu, Yong Xia, and Dinggang Shen. 2021. Disease-image-specific learning for diagnosis-oriented neuroimage synthesis with incomplete multi-modality data. *IEEE Transactions on Pattern Analysis and Machine Intelligence* (2021).

[78] Gemma Piella and Henk Heijmans. 2003. A new quality metric for image fusion. *Proceedings 2003 International Conference on Image Processing (Cat. No. 03CH37429)* 3, III–173.

[79] Jianyang Qin, Lunke Fei, Zheng Zhang, Jie Wen, Yong Xu, and David Zhang. 2022. Joint specifics and consistency hash learning for large-scale cross-modal retrieval. *IEEE Transactions on Image Processing* 31 (2022), 5343–5358.

[80] Yili Qu, Chufu Deng, Wanqi Su, Ying Wang, Yutong Lu, and Zhiguang Chen. 2020. Multimodal brain MRI translation focused on lesions. *Proceedings of the 12th International Conference on Machine Learning and Computing*, 352–359.

[81] Snehashis Roy, Aaron Carass, and Jerry L Prince. 2013. Magnetic resonance image example-based contrast synthesis. *IEEE Transactions on Medical Imaging* 32 (2013), 2348–2363.

[82] Ron Rubinstein, Alfred M Bruckstein, and Michael Elad. 2010. Dictionaries for sparse representation modeling. *Proc. IEEE* 98, 6 (2010), 1045–1057.

[83] Daniel Rueckert, Luke I Sonoda, Carmel Hayes, Derek LG Hill, Martin O Leach, and David J Hawkes. 1999. Nonrigid registration using free-form deformations: application to breast MR images. *IEEE Transactions on Medical Imaging* 18, 8 (1999), 712–721.

[84] Ramprasaath R. Selvaraju, Abhishek Das, Ramakrishna Vedantam, Michael Cogswell, Devi Parikh, and Dhruv Batra. 2019. Grad-CAM: visual explanations from deep networks via gradient-based localization. *International Journal of Computer Vision* 128 (2019), 336–359.

[85] Anmol Sharma and G. Hamarneh. 2020. Missing MRI pulse sequence synthesis using multi-modal generative adversarial network. *IEEE Transactions on Medical Imaging* 39 (2020), 1170–1183.

[86] Liyue Shen, Wentao Zhu, Xiaosong Wang, Lei Xing, John M. Pauly, Baris Turkbey, Stephanie A. Harmon, Thomas Sanford, Sherif Mehralivand, Peter L. Choyke, Bradford J. Wood, and Daguang Xu. 2021. Multi-domain image completion for random missing input data. *IEEE Transactions on Medical Imaging* 40 (2021), 1113–1122.

[87] Hoo-Chang Shin, Alvin Ihsani, Ziyue Xu, Swetha Mandava, Sharath Turuvekere Sreenivas, Christopher Forster, Jiook Cha, and Alzheimer's Disease Neuroimaging Initiative. 2020. GANDALF: Generative adversarial networks with discriminator-adaptive loss fine-tuning for Alzheimer's

disease diagnosis from MRI. *International Conference on Medical Image Computing and Computer-Assisted Intervention*.

[88] Md Mahfuzur Rahman Siddiquee, Zongwei Zhou, Nima Tajbakhsh, Ruibin Feng, Michael B. Gotway, Yoshua Bengio, and Jianming Liang. 2019. Learning fixed points in generative adversarial networks: from image-to-image translation to disease detection and localization. *Proceedings of the IEEE/CVF International Conference on Computer Vision* (2019), 191–200.

[89] Rebecca L. Siegel, Kimberly D Miller, and Ahmedin Jemal. 2019. Cancer statistics, 2019. *CA: A Cancer Journal for Clinicians* 69 (2019).

[90] Carole H Sudre, Wenqi Li, Tom Vercauteren, Sebastien Ourselin, and M Jorge Cardoso. 2017. Generalised dice overlap as a deep learning loss function for highly unbalanced segmentations. Springer, 240–248.

[91] Liyan Sun, Jiexiang Wang, Yue Huang, Xinghao Ding, Hayit Greenspan, and John William Paisley. 2020. An adversarial learning approach to medical image synthesis for lesion detection. *IEEE Journal of Biomedical and Health Informatics* 24 (2020), 2303–2314.

[92] Devavrat Tomar, Manana Lortkipanidze, Guillaume Vray, Behzad Bozorgtabar, and Jean-Philippe Thiran. 2021. Self-attentive spatial adaptive normalization for cross-modality domain adaptation. *IEEE Transactions on Medical Imaging* 40 (2021), 2926–2938.

[93] Dmitry Ulyanov, Vadim Lebedev, Andrea Vedaldi, and Victor Lempitsky. 2016. Texture networks: Feed-forward synthesis of textures and stylized images. *arXiv preprint arXiv:1603.03417* (2016).

[94] David C Van Essen, Stephen M Smith, Deanna M Barch, Timothy EJ Behrens, Essa Yacoub, Kamil Ugurbil, Wu-Minn HCP Consortium, et al. 2013. The WU-Minn human connectome project: an overview. *Neuroimage* 80 (2013), 62–79.

[95] Pascal Vincent, Hugo Larochelle, Yoshua Bengio, and Pierre-Antoine Manzagol. 2008. Extracting and composing robust features with denoising autoencoders. *Proceedings of the 25th International Conference on Machine Learning*, 1096–1103.

[96] Danyang Wang, Yawen Huang, and Alejandro F Frangi. 2017. Region-enhanced joint dictionary learning for cross-modality synthesis in diffusion tensor Imaging. *International Conference on Medical Image Computing and Computer-Assisted Intervention*.

[97] Jinbao Wang, Guoyang Xie, Yawen Huang, Jiayi Lyu, Feng Zheng, Yefeng Zheng, and Yaochu Jin. 2023. FedMed-GAN: Federated domain translation on unsupervised cross-modality brain image synthesis. *Neurocomputing* 546 (2023), 126282.

[98] Jinbao Wang, Guoyang Xie, Yawen Huang, Yefeng Zheng, Yaochu Jin, and Feng Zheng. 2022. FedMed-ATL: misaligned unpaired cross-modality neuroimage synthesis via affine transform loss. *Proceedings of the 30th ACM International Conference on Multimedia* (2022).

[99] Li Wang, Yaozong Gao, Feng Shi, Gang Li, John H Gilmore, Weili Lin, and Dinggang Shen. 2015. LINKS: Learning-based multi-source integration framework for segmentation of infant brain images. *Neuroimage* 108 (2015), 160–172.

[100] Shenlong Wang, Lei Zhang, Yan Liang, and Quan Pan. 2012. Semi-coupled dictionary learning with applications to image super-resolution and photo-sketch synthesis. *Proceedings of the IEEE/CVF Conference on Computer Vision and Pattern Recognition*, 2216–2223.

[101] Yan Wang, Luping Zhou, Lei Wang, Biting Yu, Chen Zu, David S. Lalush, Weili Lin, Xi Wu, Jiliu Zhou, and Dinggang Shen. 2018. Locality adaptive multi-modality GANs for high-quality PET image synthesis. *International Conference on Medical Image Computing and Computer-Assisted Intervention* 11070 (2018), 329–337.

[102] Yan Wang, Luping Zhou, Biting Yu, Lei Wang, Chen Zu, David S. Lalush, Weili Lin, Xi Wu, Jiliu Zhou, and Dinggang Shen. 2019. 3D auto-context-based locality adaptive multi-modality GANs for PET synthesis. *IEEE Transactions on Medical Imaging* 38 (2019), 1328–1339.

[103] Zhou Wang and Alan C Bovik. 2002. A universal image quality index. *IEEE Signal Processing Letters* 9, 3 (2002), 81–84.

[104] Zhou Wang, Alan C Bovik, Hamid R Sheikh, and Eero P Simoncelli. 2004. Image quality assessment: from error visibility to structural similarity. *IEEE Transactions on Image Processing* 13, 4 (2004), 600–612.

[105] Wen Wei, Emilie Poirion, Benedetta Bodini, Stanley Durrleman, Nicholas Ayache, Bruno Stankoff, and Olivier Colliot. 2018. Learning myelin content in multiple sclerosis from multimodal MRI through adversarial training. *International Conference on Medical Image Computing and Computer-Assisted Intervention*.

[106] Jay West, J Michael Fitzpatrick, Matthew Y Wang, Benoit M Dawant, Calvin R Maurer Jr, Robert M Kessler, Robert J Maciunas, Christian Barillot, Didier Lemoine, Andre Collignon, et al. 1997. Comparison and evaluation of retrospective intermodality brain image registration techniques. *Journal of Computer Assisted Tomography* 21, 4 (1997), 554–568.

[107] Bingyu Xin, Yifan Hu, Yefeng Zheng, and Hongen Liao. 2020. Multi-modality generative adversarial networks with tumor consistency loss for brain MR image synthesis. *IEEE 17th International Symposium on Biomedical Imaging* (2020), 1803–1807.

[108] Heran Yang, Jian Sun, Aaron Carass, Can Zhao, Junghoon Lee, Jerry L Prince, and Zongben Xu. 2020. Unsupervised MR-to-CT synthesis using structure-constrained CycleGAN. *IEEE Transactions on Medical Imaging* 39 (2020), 4249–4261.

[109] Heran Yang, Jian Sun, Liwei Yang, and Zongben Xu. 2021. A unified hyper-GAN model for unpaired multi-contrast MR Image translation. *International Conference on Medical Image Computing and Computer-Assisted Intervention*.

[110] Jianchao Yang, Zhaowen Wang, Zhe Lin, Scott Cohen, and Thomas Huang. 2012. Coupled dictionary training for image super-resolution. *IEEE Transactions on Image Processing* 21, 8 (2012), 3467–3478.

[111] Jianchao Yang, John Wright, Thomas S Huang, and Yi Ma. 2010. Image super-resolution via sparse representation. *IEEE Transactions on Image Processing* 19, 11 (2010), 2861–2873.

[112] Qianye Yang, Nannan Li, Zixu Zhao, Xingyu Fan, EC Chang, Yan Xu, et al. 2018. Mri image-to-image translation for cross-modality image registration and segmentation. *arXiv preprint arXiv:1801.06940* (2018).

[113] Qianye Yang, Nannan Li, Zixu Zhao, Xingyu Fan, Eric I Chang, Yan Xu, et al. 2020. MRI cross-modality image-to-image translation. *Scientific reports* 10, 1 (2020), 1–18.

[114] Dong Hye Ye, Darko Zikic, Ben Glocker, Antonio Criminisi, and Ender Konukoglu. 2013. Modality propagation: coherent synthesis of subject-specific scans with data-driven regularization. *International Conference on Medical Image Computing and Computer-Assisted Intervention* 16 Pt 1 (2013), 606–13.

[115] Xin Yi, Ekta Walia, and Paul S. Babyn. 2019. Generative adversarial network in medical imaging: a review. *Medical Image Analysis* 58 (2019), 101552.

[116] Biting Yu, Luping Zhou, Lei Wang, Jurgen Fripp, and Pierrick T. Bourgeat. 2018. 3D cGAN based cross-modality MR image synthesis for brain tumor segmentation. *2018 IEEE 15th International Symposium on Biomedical Imaging* (2018), 626–630.

[117] Biting Yu, Luping Zhou, Lei Wang, Yinghuan Shi, Jurgen Fripp, and Pierrick T. Bourgeat. 2020. Sample-adaptive GANs: linking global and local mappings for cross-modality MR image synthesis. *IEEE Transactions on Medical Imaging* 39 (2020), 2339–2350.

[118] Ziqi Yu, Yuting Zhai, Xiaoyang Han, Tingying Peng, and Xiao-Yong Zhang. 2021. MouseGAN: GAN-based multiple MRI modalities synthesis and segmentation for mouse brain structures. *International Conference on Medical Image Computing and Computer-Assisted Intervention*.

[119] Mahmut Yurt, Salman Ul Hassan Dar, Aykut Erdem, Erkut Erdem, and Tolga Çukur. 2021. mustGAN: multi-stream generative adversarial networks for MR image synthesis. *Medical Image Analysis* 70 (2021), 101944.

[120] Matthew D. Zeiler, Dilip Krishnan, Graham W. Taylor, and Rob Fergus. 2010. Deconvolutional networks. *Proceedings of the IEEE/CVF Conference on Computer Vision and Pattern Recognition* (2010), 2528–2535.

[121] Guodong Zeng and Guoyan Zheng. 2019. Hybrid generative adversarial networks for deep MR to CT synthesis using unpaired data. *International Conference on Medical Image Computing and Computer-Assisted Intervention*.

[122] Jin Zhang, Xiaohai He, Linbo Qing, Feng Gao, and Bin Wang. 2022. BPGAN: Brain PET synthesis from MRI using generative adversarial network for multi-modal Alzheimer's disease diagnosis. *Computer Methods and Programs in Biomedicine* 217 (2022), 106676.

[123] Min Zhang, You Ni, Qinming Zhou, Lu He, Huanyu Meng, Yining Gao, Xinyun Huang, Hongping Meng, Peihan Li, Mei lian Chen, Danni Wang, J Hu, Qiu Huang, Yao Li, Fabien Chauveau, Biao Li, and Sheng Chen. 2021. 18F-florbetapir PET/MRI for quantitatively monitoring myelin loss and recovery in patients with multiple sclerosis: A longitudinal study. *EClinicalMedicine* 37 (2021).

[124] Zheng Zhang, Luyao Liu, Yadan Luo, Zi Huang, Fumin Shen, Heng Tao Shen, and Guangming Lu. 2020. Inductive structure consistent hashing via flexible semantic calibration. *IEEE Transactions on Neural Networks and Learning Systems* 32, 10 (2020), 4514–4528.

[125] Zheng Zhang, Li Liu, Fumin Shen, Heng Tao Shen, and Ling Shao. 2018. Binary multi-view clustering. *IEEE Transactions on Pattern Analysis and Machine Intelligence* 41, 7 (2018), 1774–1782.

[126] Zheng Zhang, Haoyang Luo, Lei Zhu, Guangming Lu, and Heng Tao Shen. 2022. Modality-invariant asymmetric networks for cross-modal hashing. *IEEE Transactions on Knowledge and Data Engineering* 35, 5 (2022), 5091–5104.

[127] Zizhao Zhang, L. Yang, and Yefeng Zheng. 2018. Translating and segmenting multimodal medical volumes with cycle-and shape-consistency generative adversarial network. *Proceedings of the IEEE/CVF Conference on Computer Vision and Pattern Recognition* (2018), 9242–9251.

[128] Xingzhong Zhao and Xing-Ming Zhao. 2020. Deep learning of brain magnetic resonance images: A brief review. *Methods* (2020).

[129] Bo Zhou, Chi Liu, and James S. Duncan. 2021. Anatomy-constrained contrastive learning for synthetic segmentation without ground-truth. *International Conference on Medical Image Computing and Computer-Assisted Intervention*.

[130] Bo Zhou, Rui Wang, Ming kai Chen, Adam P. Mecca, Ryan S. O'Dell, Christopher H. van Dyck, Richard E. Carson, James S. Duncan, and Chi Liu. 2021. Synthesizing multi-tracer PET images for Alzheimer's disease patients using a 3D unified anatomy-aware cyclic adversarial network. *International Conference on Medical Image Computing and Computer-Assisted Intervention*.

[131] Tao Zhou, H. Fu, Geng Chen, Jianbing Shen, and Ling Shao. 2020. Hi-Net: Hybrid-Fusion network for multi-modal MR image synthesis. *IEEE Transactions on Medical Imaging* 39 (2020), 2772–2781.

[132] Jun-Yan Zhu, Taesung Park, Phillip Isola, and Alexei A. Efros. 2017. Unpaired Image-to-Image Translation Using Cycle-Consistent Adversarial Networks. *Proceedings of the IEEE/CVF International Conference on Computer Vision* (2017), 2242–2251.

[133] Qing Zuo, Jianping Zhang, and Yin Yang. 2021. DMC-Fusion: Deep multi-cascade fusion with classifier-based feature synthesis for medical multi-modal images. *IEEE Journal of Biomedical and Health Informatics* 25 (2021), 3438–3449.